



Optimal dispatching of electric vehicles for providing charging on-demand service leveraging charging-on-the-move technology

Jiahua Qiu, Lili Du*

Department of Civil and Coastal Engineering, University of Florida, Gainesville, FL 32608, United States



ARTICLE INFO

Keywords:

Electric vehicles
Mobile vehicle-to-vehicle charging
Vehicle routing problem

ABSTRACT

Range anxiety and charging infrastructure scarcity have been the main challenges for the mass adoption of electric vehicles (EVs). The emerging mobile electric-vehicle-to-electric-vehicle (mEV) charging technology offers a promising solution, which combines battery-to-battery and connected and autonomous vehicle technologies to enable an EV with an extra battery to charge another EV *on the move*. This paper focuses on the efficient pairing and routing of electricity providers (EPs) to demand (EDs) by extending the existing Charging-as-a-Service (CaaS) strategy to the mEV charging service (referred to as CaaS⁺). We investigate the EP fleet management problem, which is mathematically modeled as a vehicle routing problem (i.e., mEV-VRP), aiming to optimally dispatch the minimum number of EPs to approach and serve the EDs. To adapt mEV charging strategy to the online service involving large-scale EDs in practice, we develop a Clustering-aid Decomposition and Merging (c-DM) algorithm. It clusters the EDs according to their coalition potential so that we can decompose a large-scale mEV-VRP into smaller subproblems which can be efficiently solved by parallel computing. Our numerical experiments built upon citywide (Chicago) and statewide (Florida) case studies confirm the efficiency of the proposed c-DM algorithm. It enables us to investigate the performance of CaaS⁺ under a realistic large-scale setup. The results show that CaaS⁺ will be applied in different proportions of EV flows to save EDs' travel time and mitigate traffic congestion to different extents in different network congestion and charging station coverage scenarios. The sensitivity analyses of EDs' energy inventory and range anxiety also provide some hints and suggestions for improving the service efficiency of CaaS⁺.

1. Introduction

The transportation system accounted for the largest portion (28 %) of greenhouse gas (GHG) emissions in the United States in 2018. The majority of the emissions are related to internal combustion engine vehicles (EPA, 2013). Accordingly, governments around the world have provided subsidies on both demand and supply sides (Foundation and Company, 2014) to promote the usage of battery-powered electric vehicles (EVs), since they show great potential to reduce oil dependence and the associated carbon emissions. However, more recent studies (Finance, 2021; Hao et al., 2020) have shown that EV usage in different countries worldwide remains at an early market stage. It will take a long transition period, around 15 to 20 years, to increase from the current market share of less than 10 % to around 60 %, depending on the region or country studied. The main challenges that discourage the mass adoption of EVs

* Corresponding author.

E-mail addresses: jq22@ufl.edu (J. Qiu), lilidu@ufl.edu (L. Du).

Table 1

Comparison between different solutions for range anxiety.

Charging Solutions	Charging technique	Recharge delay	Detour delay	Infrastructure cost	Battery standar-dization	Congestion effect	Energy save (+)/loss (-)
Level 3 charging stations	Vehicle-to-grid	≥ 30 min	Yes	N* \$50,000 (N: number of chargers; Huang and Kockelman, 2020)	Not required	(-) introduce detour traffic	(-): from detour
Electrified road	Dynamic wireless charging	Minor	Yes	\$1.1 - \$2.8 million per kilometer (Hannon, 2021)	Not required	(-) reduce road capacity	(-): low power transfer rate
BaaS/BS stations	Battery swapping	3 min for battery swapping (NIO, n.d.)	BaaS: No BS: Yes	BaaS: fleet investment: (\$50,000 per vehicle) BS: station and automated BS machinery	Required	BaaS: (+): save detour traffic (-): introduce BSV fleet BS: (-) introduce detour traffic	(+): save detour energy (-): BSVs' idle trips
CaaS (dispatching MC)	Battery-to-battery charging	≥ 30 min	No	Fleet investment: about \$50,000 per vehicle	Not required	(+): save detour traffic (-): introduce MC fleet	(+): save detour energy (-): MCs' idle trips
CaaS ⁺ (dispatching CAV EPs)	Battery-to-battery charging and CAV (mE2)	Minor	No	Fleet investment: about \$50,000 per vehicle	Not required	(+): save detour traffic (-): introduce EP fleet	(+): save detour energy (-): EPs' idle trips

include insufficient roadside recharging infrastructure, ‘range anxiety’ resulting from the limited driving range and long charging period. In recent years, the state of the art shows that we cannot enlarge battery capacity ([Wu et al., 2020](#)). And it still takes about 30 min (much longer than gas filling) to fully charge an EV battery, even with Level-3 charging stations ([Roberts et al., 2017](#)). Even though EVs can have a maximum driving distance around 200 miles, EV commuters need to plan the trips and arrange daily home charging or workplace charging carefully due to the shortage of roadside charging infrastructures. Long-distance travelers worry about limited accessibility to charging stations along intercity roads and in rural areas. Moreover, low-income communities with most residents living in apartments are less likely to install sufficient fast charging infrastructures due to limited private parking spaces or garages. As a result, EV users lack flexibility in planning their trips due to these range limits and insufficient charging facilities. Therefore, EV users need better access to roadside charging services.

Many solutions have been proposed to provide roadside charging services. We summarize them and compare their pros and cons in [Table 1](#). The state of the art shows that each solution suffers from certain limitations, and there is no perfect solution yet. A brute force solution is to build dense charging stations to extend driving range and service coverage; however, this still involves charging delays and detours as well as the associated energy losses and traffic congestion, not to mention the high infrastructure cost to ensure sufficient service coverage. Building embedded electrified roads (i.e., dynamic wireless charging) enables charging on the move in order to cut down on charging and detour delays ([Ngo et al., 2020](#)), but it is very costly (approximate \$1.1 to \$2.8 million per kilometer ([Hannon, 2021](#))). Moreover, it may reduce road capacity and worsen traffic. The battery-as-a-service (BaaS) model ([Lu and Zhou, 2013](#); [Raeesi and Zografos, 2020](#); [Shao et al., 2017](#)), which swaps batteries for EVs by dispatching battery swapping vans (BSVs), addresses the above issues but brings up the difficult issues of battery ownership and incompatibility in practical implementation ([Tang et al., 2020](#)). As a result, it is not well accepted in the USA ([Ulrich, 2021](#)), even though it is widely used in some countries such as China.

Recent advances in battery-to-battery charging technology allow vehicle-to-vehicle electricity sharing through wireless charging ([González et al., 2021](#); [Joseph and Elangovan, 2021](#); [Maglaras et al., 2014](#); [Nezamuddin and dos Santos, 2020](#); [Yan et al., 2020](#)) or cable converter assembly ([Bulut and Kisacikoglu, 2017](#); [Huang et al., 2014](#); [LLC, 2019](#); “Mobi EV Charger,” n.d.; [Umesh et al., 2021](#)). The state of the art indicates that cable assembly charging can reach a power transfer rate of up to 50 kW ([Abdolmaleki et al., 2019](#); [Afshar et al., 2021](#); [Ucer et al., 2019](#); [Umesh et al., 2021](#)). These technologies have initiated the Charging-as-a-Service (CaaS) business (e.g., BoostEV ([Morris, 2021](#))) in practice, which dispatches Mobile Chargers (MCs) to charge EVs at designated locations and times ([Cui et al., 2018b, 2018a](#); [Huang et al., 2014](#); [Li, 2019](#); [Tang et al., 2020](#)). The current practice shows that CaaS carries similar pros and cons to those of BaaS while avoiding battery compatibility and ownership issues. However, it still cannot avoid the long charging delay.

Most recently, some studies ([Abdolmaleki et al., 2019](#); [Chakraborty et al., 2020](#); [Kosmanos et al., 2018](#); [Maglaras et al., 2014](#)) investigated an emerging technology – on-the-move electric-vehicle-to-electric-vehicle charging (mE2), the focus of this study – which integrates the emerging battery-to-battery charging and Connected and Autonomous Vehicle (CAV) technologies. Specifically, a pair of EVs (also CAVs) will synchronize their movement using CAV technology and then conduct on-the-move electricity sharing through the battery-to-battery charging technology. Several futuristic and promising techniques will address the safety and congestion issues regarding EV pairing. For example, CAV platooning techniques, such as Adaptive Cruise Control (ACC) and Cooperative Adaptive

Cruise Control (CACC) (Chen et al., 2019; Dey et al., 2015; Gong et al., 2016; Gong and Du, 2018; Guanetti et al., 2018; Liang et al., 2015; Ma et al., 2020; Wang et al., 2018), have been developed to synchronize the movement of CAVs on the road, which enables two vehicles to move safely in a relatively stable and small space. Advanced mechanical design also ensures the safety of connecting EV pairs. For instance, Chakraborty et al., propose a charging arm that is controlled by an autopilot system, charging port tracking, and a protection system between the EVs for charge sharing (Chakraborty et al., 2022). Vehicle modular technology addresses the safety issue using similar automated arm technologies, where the feedback control can turn on/shut down charging power and connect/retract the connection when a fault or (traffic) safety issue emerges (Chen et al., 2019).

As charging is conducted on the move, this mE2 charging technique can substantially reduce recharging delays and boost the existing abilities of CaaS and charging station service by dispatching CAV electricity providers (EPs) and conducting on-the-move charging service (mE2 charging service). We refer to this as CaaS⁺ in Table 1 to differentiate it from the exiting CaaS. Clearly, CaaS⁺ inherits the merits of CaaS and BaaS and will have great potential to promote the mass adoption of EVs by improving driver satisfaction. It can save EVs from detours/delays to/at charging stations and lessen their dependence on home or workplace charging.

Despite the benefits of CaaS⁺, this study recognizes that the EP fleet will introduce extra traffic and will potentially worsen traffic; EPs' trips will lead to energy losses, which raises the inherent operation cost and jeopardizes the energy saving potential of CaaS⁺. Similar issues also exist in BaaS and CaaS. Therefore, fleet management is one of the critical issues that need to be carefully investigated to fully take advantage of this technological advancement while avoiding its side effects.

Existing studies have recognized these issues and investigated using private EVs as EPs to provide peer-to-peer charging (Abdolmaleki et al., 2019) based on the sharing economy concept to eliminate the need for an EP fleet. This study proposes dispatching commercial EPs, on the other hand, to further expand the application of mE2 technology in the scenarios in which we cannot find sufficient private EPs, such as under low EV penetration, the spatiotemporal imbalance between private EPs and demands under high EV penetration, or EVs with emergent last-mile energy gaps. To best implement the CaaS⁺ service, this study aims to optimally dispatch the minimum number of EPs to satisfy charging requests while mitigating the traffic overhead. It is worth mentioning that the profits and costs of the mE2 charging business involve many other factors beyond the fleet management explored by this study, such as the pricing problem, and these are out of the scope of this study.

Overall, this study makes the following methodology contributions. We mathematically model the fleet dispatching problem in each batch of the CaaS⁺ service as a vehicle routing problem (referred to as mE2-VRP). Its solution provides the minimum size of the EP fleet needed to provide timely service for EDs while mitigating traffic overhead. Two critical points highlight the novelty of this VRP. First of all, the mE2-VRP model is built upon an encounter network to address trip synchronization between EPs and EDs en route. This is different from most of the existing VRP models (see our literature review for details). Next, the mE2-VRP introduces unique subtours due to on-the-move electricity delivery. More precisely, an ED moves along encounter nodes on its trip, and electricity delivery can occur to the same ED at different encounter nodes. Then the subtour can be a service tour revisiting the same ED at the same encounter node or the same ED at a different encounter node. The former is illegal since the ED is moving toward its destination and will not revisit a node, while the latter is legal since an ED can accept multiple times of service. This is different from subtours in conventional VRP models, which only consider revisiting the same demand at the same node as a subtour. Therefore, we develop new constraints to eliminate illegal subtours. Their effectiveness and correctness are mathematically proved.

We develop a Clustering-aided Decomposition and Merging (c-DM) algorithm to address the scalability difficulties of mE2-VRP in practical applications. Along with this effort, we contribute a new quantitative approach to measure the coalition potential between two EDs (i.e., whether two EDs can be served by the same EP in their trips). Based on coalition potential, we develop a customized clustering method that decomposes a large-scale mE2-VRP into multiple small subproblems. And then, we solve the subproblems efficiently and independently by parallel computing to obtain a feasible solution of the mE2-VRP. Last, we design a strategic merging algorithm that improves the feasible solution to a better solution for the mE2-VRP. The c-DM algorithm makes it possible to adapt CaaS⁺ to online applications involving large-scale ad hoc demands in practice.

Taking advantage of the computational efficiency of the c-DM algorithm, we conduct numerical studies to explore the benefits and applicability of CaaS⁺ in practical implementations. Our experimental results show that CaaS⁺ will save EDs travel time and reduce trip distance. It also helps mitigate congestion when traffic is not highly congested. In addition, the analysis of EDs range anxiety gives insight into strategies to guide EDs' energy requests to improve service efficiency. Note that without an efficient approach like the c-DM algorithm, we are not able to investigate those insights for the CaaS⁺ service implemented in a city-wide or state-wide network. Overall, this research is among the first efforts to study the application of mE2 charging technologies for EV charging on the move.

The study is organized by the following structure in the rest of the paper. Section 2 gives a literature review and Section 3 introduces CaaS⁺. Following that, we formulate the mE2-VRP in Section 4 and develop the solution methodology in Section 5. Based on the Chicago sketch network and Florida statewide network, Section 6 presents numerical experiments to validate the developed models and algorithms. Some managerial insights are also presented. Last, we present concluding remarks in Section 7.

2. Literature review

This section first provides a brief review of recent progress on EV charging services using mE2 charging techniques and explains the motivation behind our study. We next focus on discussing the most closely related VRP models and their solution methods, in order to indicate the research gaps we seek to bridge.

Existing studies show that mE2 charging can be conducted by either wireless power transfer or converter cable assembly charging technologies (Chakraborty et al., 2020; Dai and Ludois, 2014; Roberts et al., 2017). More precisely, Mou et al., indicated that the wireless power transfer efficiency of the benchmark transmitter coil reaches 80% (Mou et al., 2020), and the plug-in charging

(converter cable assembly) can achieve even higher efficiency (Mou et al., 2019). Thanks to advances in charging technology, existing studies suggest that mE2 charging techniques will be an efficient charging option and supplement to existing charging options in the future. Accordingly, several studies have already explored potential implementation strategies to promote their usage. For example, the study of Kosmanos et al., and Maglaras et al., developed a mobile charging system, in which the EPs are buses that carry high-capacity batteries (Kosmanos et al., 2018; Maglaras et al., 2014). While moving with buses, the EDs will receive energy via plug-in electric connection or via WPT (electromagnetic induction). Clearly, the fixed bus routes will limit service coverage. Another important work, developed by Abdolmaleki et al., introduced a peer-to-peer charging strategy, which routes private EVs (i.e., EPs and EDs) to enable power exchange between them for several operational merits such as reducing the cost of managing the EP fleet (Abdolmaleki et al., 2019). Experimental results show that the peer-to-peer EV charging service strategy offers significant energy and travel time saving, with 85 % demand acceptance rate if the demand-to-supplier ratio approaches one to one. Therefore, the demand acceptance rate may drop when there are not enough suppliers, since an ED may not be able to find an EP nearby in a timely manner, such as when the EV penetration is low, or when there is an imbalance between demand and supply. Accordingly, we consider another strategy: dispatching commercial EPs to serve EDs.

This study recognizes that the mE2-VRP developed in this study is closely related to two other VRP models in the literature: (i) the Dial-a-Ride-Problem (DARP) and (ii) the VRP with mobile targets (VRPMT). The DARP is a large-scale mixed-integer linear programming (MILP) that designs routes for a vehicle fleet to provide shared-ride services for customers with given travel information, e.g., origin, destination, and preferred arrival time (Cordeau and Laporte, 2007). In comparison, the mE2-VRP is a more complex problem because it involves non-stationary customers (EDs) and service delivery, thereby introducing complexity in tracking the movement of EDs and synchronizing the movement of EPs and EDs spatiotemporally. Specifically, unlike the DARP, in which the pick-up and drop-off locations are given, the mE2-VRP needs to determine when and where the EPs are to meet, move together with, and then detach from the EDs, which complicates the problem formulation.

The VRPMT and mE2-VRP, on the other hand, share the common feature of considering mobile targets but consider different service delivery patterns. The mE2-VRP provides an on-the-move charging delivery service to moving EDs, while VRPMP considers stationary delivery at a location where the vehicle and mobile target meet. Existing literature developed two typical VRPMTs. They are the VRP with roaming delivery locations (VRPRDL) (Ozbaygin et al., 2017; Reyes et al., 2017) and the VRP with floating targets (VRPFT) (Gambella et al., 2018). The VRPRDL considers that each customer will visit a set of static locations, e.g., home and workplaces, and a single stationary delivery can occur at one of these static candidate locations. In the VRPFT, customers are allowed to travel from their homes and be picked up by vehicles during the trips. But each customer is assumed to travel on a straight line with constant speed. However, the mE2-VRP addresses a multi-depot, multi-vehicle routing problem, in which EDs have their own sophisticated routes (rather than traveling only in one direction), and EP-ED pairs will run together so that electricity can be delivered on the move. Moreover, the delivery product of the mE2-VRP is electricity, which can be requested by an ED at any time with various amounts during its route. Accordingly, an ED can accept multiple times of service from different EPs during its route (i.e., partial charging is allowed at each service). These unique features make the mE2-VRP a more complicated problem than the existing VRPMTs.

Exact solution approaches, such as branch-and-cut algorithms and branch-and-price algorithms, have been used to solve DARP (Baldacci et al., 2011; Braekers et al., 2014; Parragh, 2011; Parragh and Schmid, 2013). A branch-and-price algorithm is also adopted to solve VRPRDL (Ozbaygin et al., 2017; Reyes et al., 2017). The existing literature shows that VRPRDL instances of up to 120 customers can be solved by branch-and-price. And the largest instance solved for the standard DARP involves 8 vehicles and 96 customers (Ropke et al., 2007).

Regarding heuristic approaches, several approaches have been tested for solving the DARP to fulfill its online application in the literature. They include Tabu Search (TS) (Cordeau and Laporte, 2003), Variable Neighborhood Search (VNS) (Muelas et al., 2013; Parragh et al., 2010), Deterministic Annealing (DA) (Braekers et al., 2014), and Adaptive Large Neighborhood Search (ALNS) (Masson et al., 2014), etc. These approaches often start with an initial solution and repeatedly search for better solutions according to designed strategies, such as merging trips by destroying and repairing operations. Therefore, quickly generating a good initial solution plays a key role in sustaining the efficiency of these heuristic approaches. However, there is not an apparent and efficient strategy to generate a good initial feasible solution for the mE2-VRP because the mobile customers – EDs – have their own routes, travel schedules, and energy levels. For example, a naive initial solution is to perform a one-to-one dispatch of EPs to EDs. However, starting from this solution, we still face difficulty in improving the solution by destroying the route of one EP and merging it into the other. This is because the two EDs have complicated trip schedules and battery inventories. It is very possible that their services cannot be merged and accommodated by one EP. Therefore, we need a well-designed strategy to generate the initial solution that considers the coalition potential between EDs' trips. Furthermore, we need to design a customized strategy in the search for better solutions instead of random searching as adopted by most of the existing heuristic approaches. In conclusion, the mE2-VRP calls for a new dedicated solution methodology. Our study thus develops the c-DM algorithm to address the technical difficulty for this particular application.

3. Problem description and formulation

CaaS⁺ seeks to efficiently provide an on-the-move charging service for the electric vehicles en route. Before formally formulating this problem, we should first establish assumptions. First of all, CaaS⁺ does not require an ED to detour in order to receive an electricity delivery. Instead, an ED may meet an EP and accept the electricity delivery on the move along the ED's pre-defined route. It may cause a waiting time before an ED meets the assigned EP at a location on its route. The CaaS⁺ service will satisfy each the tolerable delay reported in each ED's service request. Therefore, the CaaS⁺ service will help an ED avoid all other unwanted delays due to recharging. Moreover, by taking advantage of the mE2 charging technique, CaaS⁺ allows an ED to accept multiple times of service from different

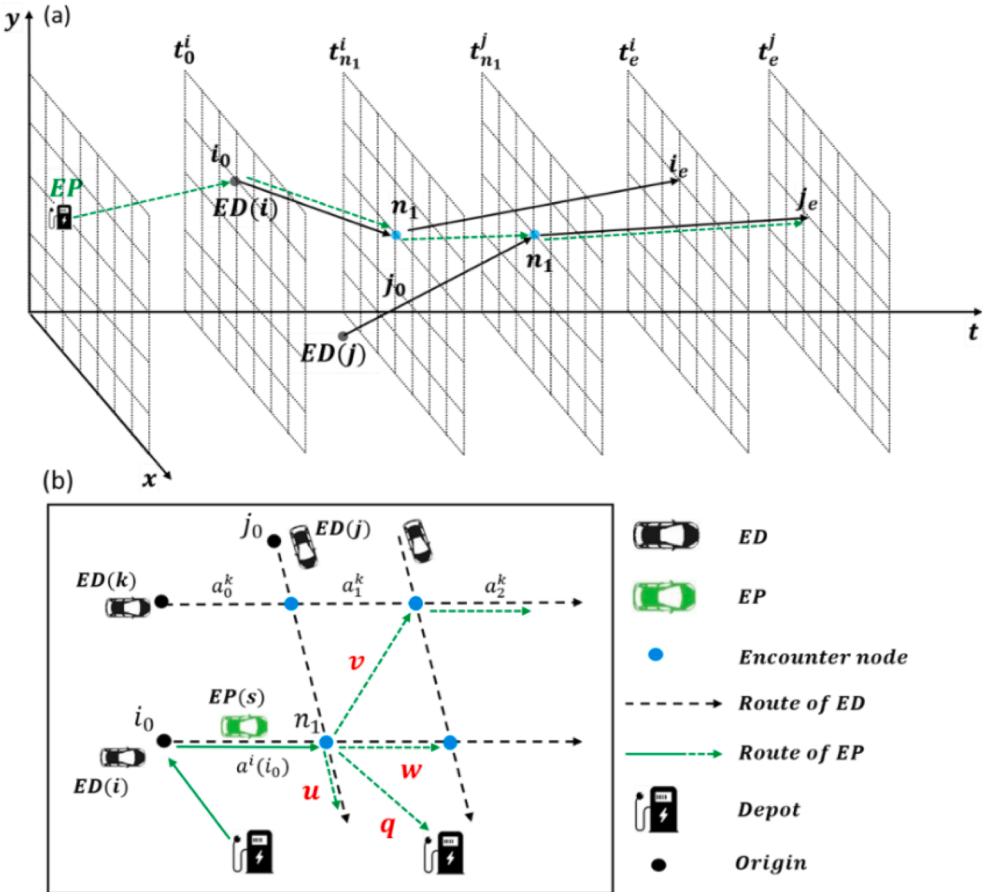


Fig. 1. Schematic representation of the mE2-VRP on a (a) spatiotemporal network and (b) simplified spatial network.

EPs at different spots along its route. This means that partial charging at each electricity delivery service is permitted. Lastly, we consider average energy consumption and travel time on each link, which is a well-accepted assumption in the literature (Bongiovanni et al., 2019; Cui et al., 2018b, 2018a; Raeisi and Zografos, 2020; Schneider et al., 2014; Tang et al., 2020). The potential mismatch between the EPs and the EDs in the routing plan resulting from this assumption can be accommodated by the demands' schedule flexibility (discussed in Section 3.2). Based on these assumptions, we will explore optimal routes for dispatching the EPs so that they can serve the EDs en route with the smallest fleet size, which helps reduce the traffic overhead introduced by the EPs. To do that, the sections below will formally define CaaS⁺, electricity suppliers, and demands.

3.1. CaaS⁺ and electricity suppliers

We first describe CaaS⁺, taking Fig. 1(a) as an example. Specifically, we consider that ED(i) can be served at the earliest at time t_0^i and location i_0 on its route. After passing location i_0 , ED(i) goes through node n_1 at the time $t_{n_1}^i$ and then arrives at destination i_e at the time t_e^i . In the meantime, an EP departs from its current location or depot and will serve an ED such as i by meeting it at a node such as i_0 and then moving together with ED(i) to distribute electricity along its route. After finishing with ED(i), the EP will continue to serve another ED if it still has enough electricity inventory. By studying the chance that an EP moves from one ED to another, we notice that those nodes where two EDs meet (such as n_1), are more attractive to schedule the mE2 service, since it potentially enables an EP to serve a new ED (such as j) without extra idle travel after it finishes with the current ED (such as i). This unique feature encourages us to build CaaS⁺ on a novel network mainly composed of the encounter nodes of EDs' routes. Then, an EP trip formed in such a network will enable this EP to meet and serve several EDs at the encounter nodes along its route. Thus, this novel network will help us to synchronize the trips of EPs and EDs. In a real road network, a route is a collection of links. The encounter nodes are determined by EDs' routes. They can be either overlapped links along the routes or intersections of routes. In practice, given that an EP meets the two EDs at an encounter node for a charging service switch such as from ED-a to ED-b, we consider the following three implementation scenarios. (i) If the encounter node is an overlapped link and ED-b does not need to wait for the EP, then ED-b can directly meet the EP without parking. (ii) If the encounter node is an overlapped link and ED-b needs to wait for the EP, then ED-b can park and wait in a nearby parking lot, road shoulder (if parking is allowed), or rest area on the highway. (iii) If the encounter node is an intersection, then ED-b

would meet EP at a nearby parking space. Please see Appendix B for a detailed discussion of the algorithm to build the encounter network.

Consequently, we consider a directed graph $G(\mathcal{N}, A)$ with the node set $\mathcal{N} = N \cup N_0 \cup N_e \cup N_p$ and the arc set A (see Fig. 1(b) for an example). Specifically, N includes all the encounter nodes between the EDs. N_0 represents the set of the first available locations along the itineraries of the EDs, where the strategy can provide the earliest CaaS⁺ service. N_e represents the set of the destinations of the EDs. N_p contains the current locations of the available EPs (which can be depots or the current locations of the idle EPs). Each arc $(n, m) \in A, \forall n, m \in \mathcal{N}, n \neq m$ in the graph $G(\mathcal{N}, A)$ represents a route connecting two nodes in the physical map. Note that a physical route may involve multiple roads which are not presented in the graph $G(\mathcal{N}, A)$. Each arc in G has an associated average travel time $t_{n \rightarrow m}$ and energy cost $e_{n \rightarrow m}$. The visiting time stamps of each ED at the nodes on its route are recorded by a set of continuous variables, which will be introduced later.

Next, we consider a set of EPs denoted by \mathcal{S} . They are either parked in their respective depots or idle along their routes after completing their services in the last batch. For each EP(s), $\forall s \in \mathcal{S}$, we denote its initial energy inventory by e_0^s , its current location by s_0 , and its energy consumption rate by ϖ_s . We also let $e_{n \rightarrow m}^-, \forall n, m \in \mathcal{N}$ represent the average energy consumption for an EP traveling on the path from node n to m involving several arcs in $G(\mathcal{N}, A)$, which can be estimated by the EP's energy consumption rate and the average route travel time. This study discretizes the service horizon, i.e., one day, into a set H of time intervals, with interval length T , i.e., 30 min. Accordingly, we denote $\mathcal{D}_h, \forall h \in H$, as a batch of the EDs that send the CaaS⁺ service requests within the h -th time interval. We further assume that at the beginning of each time interval, h , the total energy storage of the available EPs is sufficient to serve all energy requests; if not, excess EDs will be declined and then transferred to the next batch so that our model can fit. The strategy solves the mE2-VRP once for each batch and then dispatches a fleet of EPs to serve the EDs in \mathcal{D}_{h-1} . For convenience, we abbreviate \mathcal{D}_h as \mathcal{D} for the rest of the paper, since the approach is adaptive to each time interval $h \in H$. As the strategy is operated under a rolling horizon, the solution time of the mE2-VRP is required to be smaller than the interval length T , which calls for an efficient solution algorithm.

3.2. Electricity demands en route

We next define the features of the electricity demands. After collecting electricity requests from the EDs, CaaS⁺ takes a tolerant service lead time to process the requests and dispatch EP services. Accordingly, ahead of the lead time, each ED(i) is required to provide (1) its battery features (capacity \bar{e}_i and energy consumption rate ϖ_i), and (2) its origin–destination pair (i_0, i_e) , endurable waiting time, and the route it selects, such as a route suggested by a navigation apps. Here, the origin i_0 is the first location that the ED is available to accept the service. Specifically, the first service location, i_0 , can be any spot en route or even at the origin if the ED does not depart. In addition, the system needs information regarding its estimated arrival time (\tilde{t}_0^i) and battery level (e_0^i). Moreover, this study considers that individual EDs propose their endurable waiting time $\bar{\tau}_i$ at their origin i_0 as they request the service. $\bar{\tau}_i$ can be zero, or logically a shorter time than the detour and charging time to the nearest charging station. Otherwise, EDs wouldn't call for the CaaS⁺ service.

With the given information from the EDs, the system maps the route of each ED to the graph $G(\mathcal{N}, A)$ by a tuple of nodes, i.e., $\mathcal{N}_i = (i_0, N_i, i_e), i \in \mathcal{D}$, where N_i represents the encounter nodes along the route of ED (i). Moreover, we use t_n^i to represent the departure time of ED(i) at node $n \in \mathcal{N}_i$. Assuming each ED(i) is only willing to wait for service at the origin i_0 , we can estimate its departure time from i_0 by $t_0^i = \tilde{t}_0^i + \tau_i$, where the waiting time τ_i satisfies $0 \leq \tau_i \leq \bar{\tau}_i$. Accordingly, along the route of ED(i) on the graph $G(\mathcal{N}, A)$, we have the relation $t_n^i = t_0^i + t_{i_0 \rightarrow n} = \tilde{t}_0^i + t_{i_0 \rightarrow n} + \tau_i, \forall i \in \mathcal{D}, n \in \mathcal{N}_i$, where $t_{i_0 \rightarrow n}$ represents the average travel time from location i_0 to node n along the route on $G(\mathcal{N}, A)$. The set of the EDs passing through a node n is denoted by $D_n, n \in \mathcal{N}$.

To facilitate the development of our mathematical model, this study also describes the route of each ED(i) on $G(\mathcal{N}, A)$ by the arcs involved. Accordingly, we let $A_i = \{a_n^i\}_{n \in \mathcal{N}_i} \subseteq A$ denote the route of ED(i), where a_n^i represents an arc starting from node n on the route of ED(i). To simplify the presentation, a_n^i is replaced by $a^i(n)$ in some formulations. Fig. 1(b) demonstrates how two different ways are used to denote the arc for ED(i) and ED(k), respectively. We further introduce continuous variables $e_{i,a}^+, i \in \mathcal{D}, a \in A_i$ to represent the electricity delivered to ED(i) on the arc a . Correspondingly, we use parameters $e_{i,a}^-, i \in \mathcal{D}, a \in A_i$ to represent the energy loss of ED(i) along the arc a . Note that we consider $e_{i,a}^-$ as a known parameter that can be estimated by the given terrain type, distance, and average travel time, among other factors affecting EVs' energy consumption.

3.3. Encountering and switching schemes

This study considers that an EP(s) can meet an ED(j) at either its origin node or any encounter nodes, and then follows ED(j) on the arc $a \in A_j$ to deliver the electricity until the next node, with a known power transfer rate η . If EP(s) has enough energy once it arrives at the next node, EP(s) can continue to charge ED(j); or it can either switch to serve another ED(j) at the current node (local customer switch, referred to as local switch hereafter) or drives to serve another ED(k) at different node (distant customer switch, referred to as distant switch hereafter). If EP(s) does not have enough energy, it will return to a depot. Also, along any arc $a \in A$, we assume the EP(s) can charge at most one ED at a time. To model these decision actions involved in this CaaS⁺ service, we introduce a set of binary planning variables as follows.

$$z_{i,a}^s = \begin{cases} 1 & \text{if EP}(s) \text{ serves ED}(i) \text{ on the arc } a \in A_i, \forall s \in \mathcal{S}, i \in \mathcal{D}, a \in A_i \\ 0 & \text{otherwise} \end{cases}$$

$$\begin{aligned}
o_i^{n,s} &= \begin{cases} 1 & \text{if } EP(s) \text{ travels from a depot} \\ & \text{to charge } ED(i) \text{ at node } n, \forall s \in \mathcal{S}, i \in \mathcal{D}, n \in \mathcal{N}_i \setminus i_e \\ & 0 \text{ otherwise} \end{cases} \\
q_i^{n,s} &= \begin{cases} 1 & \text{if } EP(s) \text{ leaves } ED(i) \text{ and} \\ & \text{return to depot from node } n, \forall s \in \mathcal{S}, i \in \mathcal{D}, n \in \mathcal{N}_i \setminus i_0 \\ & 0 \text{ otherwise} \end{cases} \\
u_{i,j}^{n,s} &= \begin{cases} 1 & \text{if } EP(s) \text{ conducts local switches} \\ & \text{from } ED(i) \text{ to } ED(j) \text{ at node } n, \forall s \in \mathcal{S}, i \in \mathcal{D}, n \in \mathcal{N}_i \setminus i_0, j \in D_n, j \neq i \\ & 0 \text{ otherwise} \end{cases} \\
v_{i,j}^{n,m,s} &= \begin{cases} 1 & \text{if } EP(s) \text{ conducts distant switches from} \\ & ED(i) \text{ at node } n \text{ to } ED(j) \text{ at node } m, \forall s \in \mathcal{S}, i, j \in \mathcal{D}, i \neq j, n \in \mathcal{N}_i \setminus i_0, m \in \mathcal{N}_j \setminus j_e, n \neq m \\ & 0 \text{ otherwise} \end{cases} \\
w_i^{n,s} &= \begin{cases} 1 & \text{if } EP(s) \text{ charges } ED(i) \text{ on arc } a^i(n) - 1 \\ & \text{and continue to charge } ED(i) \text{ on arc } a^i(n), \forall s \in \mathcal{S}, i \in \mathcal{D}, n \in N_i \\ & 0 \text{ otherwise} \end{cases}
\end{aligned}$$

Based on the above problem setup, we try to find optimal schemes to match and route the EPs to the EDs so that they meet and conduct the electricity charging when they are on the move. For example, in Fig. 1(a), EP(s) firstly charges ED(i) from node i_0 to node n_1 . Then EP(s) waits $t_{n_1}^i - t_{i_0}^i$ units of time at node n_1 (i.e., wait at nearby roadside spaces), switches the charging target to ED(j) and continues to charge ED(j) until its destination i_e . To generate an optimal schedule for CaaS⁺ to dispatch the EPs, we develop a mE2-VRP model, which is a large-scale MILP, and solve it by a heuristic solution approach called c-DM algorithm. We discuss the technical details of these methods in the following sections. All variables and parameters used within the formulation and the algorithm are summarized in Table 3 in Appendix A.

4. Mathematical formulation

CaaS⁺ raises a VRP problem for the electricity delivery between two mobile electric vehicles (i.e., mE2-VRP). Mathematically we formulated the mE2-VRP as a MILP from Equation (1) to Equation (15), which explores the optimal routing plans for the EPs to serve a set of EDs subject to their energy availability and charging requests, while minimizing the EP fleet size (Equation (1)). Accordingly, the current objective function in Equation (1) seeks to minimize the fleet size of the EPs. To be noted, the objective function can also be extended to minimize the total travel costs or idle energy losses without introducing extra complexity to our algorithm design (see Section 4). The development of the constraints considers the following aspects: flow conservation of the EPs ensured by the constraint set (2)-(7); the feasible energy inventory of EPs and EDs are ensured by the constraints (8)-(12). Last, constraints (13) and (14) enable the temporal-feasibility of a local/distant switch and they eliminate the illegal subtours of the EPs. Validity of those constraints are discussed in detail in the following subsections.

mE2-VRP

$$\min F(O) = \sum_{s \in \mathcal{S}} \sum_{i \in \mathcal{D}} \sum_{n \in \mathcal{N}_i \setminus i_e} o_i^{n,s} \quad (1)$$

subject to

$$\sum_{\substack{j \in D_n \\ j \neq i}} u_{i,j}^{n,s} + \sum_{\substack{j \in D \\ j \neq i}} \sum_{m \in \mathcal{N}_j \setminus j_e} v_{i,j}^{n,m,s} + w_i^{n,s} + q_i^{n,s} = z_{i,a^i(n)-1}^s, \quad \forall s \in \mathcal{S}, i \in \mathcal{D}, n \in N_i \quad (2)$$

$$\sum_{\substack{j \in D_n \\ j \neq i}} u_{j,i}^{n,s} + \sum_{\substack{j \in D \\ j \neq i}} \sum_{m \in \mathcal{N}_j \setminus j_0} v_{j,i}^{m,n,s} + o_i^{n,s} + w_i^{n,s} = z_{i,a^i(n)}^s, \quad \forall s \in \mathcal{S}, i \in \mathcal{D}, n \in N_i \quad (3)$$

$$\sum_{\substack{j \in D_{i_e} \\ j \neq i}} u_{i,j}^{i_e,s} + \sum_{\substack{j \in D \\ j \neq i}} \sum_{m \in \mathcal{N}_j \setminus i_e} v_{i,j}^{i_e,m,s} + q_i^{i_e,s} = z_{i,a^i(i_e)-1}^s, \quad \forall s \in \mathcal{S}, i \in \mathcal{D} \quad (4)$$

$$\sum_{\substack{j \in D_{i_0} \\ j \neq i}} u_{j,i}^{i_0,s} + \sum_{\substack{j \in D \\ j \neq i}} \sum_{m \in \mathcal{N}_j \setminus i_0} v_{j,i}^{m,i_0,s} + o_i^{i_0,s} = z_{i,a^i(i_0)}^s, \quad \forall s \in \mathcal{S}, i \in \mathcal{D} \quad (5)$$

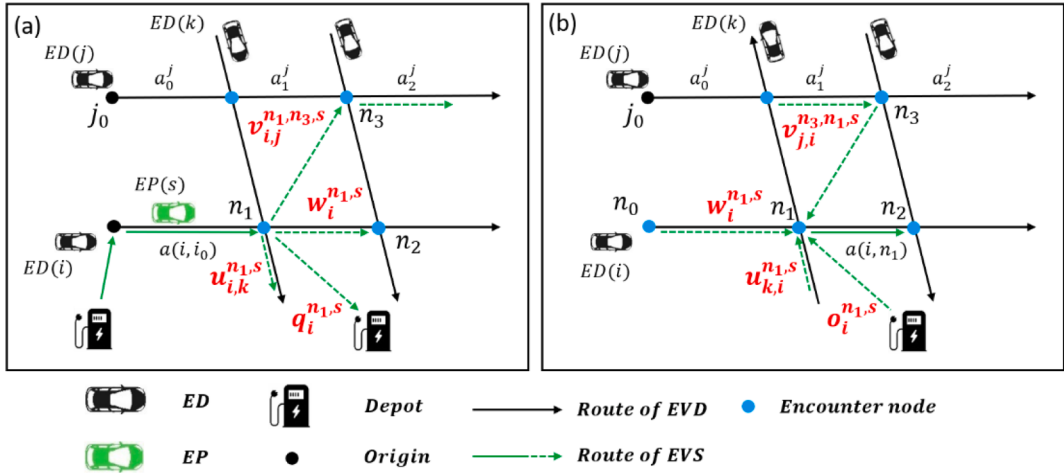


Fig. 2. Representation of the flow conservation constraints.

$$\sum_{i \in \mathcal{D}} \sum_{n \in \mathcal{N}_i \setminus i_0} o_i^{n,s} \leq 1, \quad \forall s \in \mathcal{S} \quad (6)$$

$$\sum_{i \in \mathcal{D}} \sum_{n \in \mathcal{N}_i \setminus i_0} q_i^{n,s} \leq 1, \quad \forall s \in \mathcal{S} \quad (7)$$

$$e_n^i = e_0^i + \sum_{a=a^i(i_0)}^{a^i(n)-1} e_{i,a}^+ \left(\sum_{s \in \mathcal{S}} z_{i,a}^s \right) - \sum_{a=a^i(i_0)}^{a^i(n)-1} e_{i,a}^-, \quad \forall i \in \mathcal{D}, n \in \mathcal{N}_i \setminus i_0 \quad (8)$$

$$0 \leq e_{i,a}^+ \leq \bar{e}_{i,a}^+, \quad \forall i \in \mathcal{D}, a \in A_i \quad (9)$$

$$e_{-d} \leq e_n^i \leq \bar{e}_i, \quad \forall i \in \mathcal{D}, n \in \mathcal{N}_i \setminus i_0 \quad (10)$$

$$E_s = \sum_{i \in \mathcal{D}} \sum_{n \in \mathcal{N}_i \setminus i_e} o_i^{n,s} e_{s_0 \rightarrow n}^- + \sum_{i \in \mathcal{D}} \sum_{j \in D} \sum_{n \in \mathcal{N}_i \setminus i_0} v_{i,j}^{n,m,s} e_{n \rightarrow m}^- + \sum_{i \in \mathcal{D}} \sum_{a=a^i(i_0)}^{a^i(i_e)-1} z_{i,a}^s (e_{i,a}^+ + e_{s,a}^-) + \sum_{i \in \mathcal{D}} \sum_{n \in \mathcal{N}_i \setminus i_0} q_i^{n,s} e_{n \rightarrow p_n}^- \quad (11)$$

$$e_0^s - E_s \geq e_{-s}, \quad \forall s \in \mathcal{S} \quad (12)$$

$$t_n^i - t_n^i \geq M(u_{i,j}^{n,s} - 1), \quad \forall s \in \mathcal{S}, i \in \mathcal{D}, n \in \mathcal{N}_i \setminus i_0, j \in D_n, j \neq i \quad (13)$$

$$t_m^i - t_n^i - t_{n \rightarrow m} \geq M(v_{i,j}^{n,m,s} - 1), \quad \forall s \in \mathcal{S}, i, j \in \mathcal{D}, i \neq j, c \in \mathcal{N}_i \setminus i_0, m \in \mathcal{N}_j \setminus j_e \quad (14)$$

$$t_n^i = t_0^i + t_{i_0 \rightarrow n} = \tilde{t}_0 + t_{i_0 \rightarrow n} + \tau_i, \quad \forall i \in \mathcal{D}, n \in \mathcal{N}_i \quad (15)$$

4.1. Flow conservation constraints

Constraints set (2)-(5) to ensure the EP flow conservation at each node. Mainly, constraints (2) and (4) model the actions that an EP will take at a node n . To do that, we introduce binary variables $z = \{z_{i,a}^s\}$ to indicate if there is an EP moving on the arc a . Taking Fig. 2(a) as an example, we can see that EP(s) charges ED(i) as they move together on arc $a^i(n_1) - 1$ and arrives at node n_1 . Thus, there is an EP entering node n_1 . Mathematically, it indicates that $z_{i,a^i(n_1)-1}^s = 1$ on the right side of (2). To ensure flow conservation, we should have an EP leaving node n_1 . Fig. 2(a) shows that there are four options, and EP(s) can only take one out of them. This study thus uses four binary variables on the left-hand side of constraints (2) to model this decision. Specifically, EP(s) may continue charging ED(i) toward the downstream segment, then we have $w_i^{n_1,s} = 1$; or do a local service switch from ED(i) to ED(k) at node n_1 , then we have $u_{i,k}^{n_1,s} = 1$; or do a distant service switch from ED(i) to ED(j) by traveling from node n_1 to node n_3 , then we have $v_{i,j}^{n_1,n_3,s} = 1$; or return to a depot, which means $q_i^{n_1,s} = 1$. However, if $z_{i,a^i(n_1)-1}^s = 0$ on the right side of (2), none of the four actions are feasible for EP(s) at node n_1 . The flow conservation constraints (2) make the four integer variables on the left side take zero values. Similarly, constraints (4) model the same flow conservation relationship in the case where node n_1 is the destination of ED(i), i_e . Note that variable $w_i^{n_1,s}$ is omitted in

constraints (4) because ED(i) arrives at destination and there is not a downstream arc on its route.

Similarly, constraints (3) and (5) capture all possible actions that drive an EP arriving at node n . Fig. 2(b) shows an example. If EP(s) serves ED(i) on the arc $a^i(n_1)$, then we know that there must be an EP leaving from node n_1 , which makes $z_{i,a^i(n_1)}^s = 1$ on the right side of (3). On the other hand, the left side of (3) indicates that EP(s) can arrive at node n_1 by only taking one of the four actions, which introduces four integer variables similar to what we discussed above. Namely, it may come from a depot, then we have an integer variable $o_i^{c_1,s} = 1$, or continue charging ED(i) from an upstream segment to node n_1 , then it makes $w_i^{n_1,s} = 1$; or perform a local switch from ED(k) to ED(i) at n_1 , then we have $u_{k,i}^{n_1,s} = 1$; or conduct a distant switch from ED(j) to ED(i), then we have $v_{j,i}^{n_1,n_1,s} = 1$. Clearly, if $z_{i,a^i(n_1)}^s = 0$ on the right side of (3), the constraints make the corresponding four integer variables on the right side take zero values since there is not an EP arriving at node n_1 . Similarly, this flow conservation relationship is modeled by constraints (5) when n_1 is the origin of ED(i), i_0 . In this case, there is no upstream arc to i_0 on the route of ED(i), so variable $w_i^{n_1,s}$ is omitted in constraints (5).

Furthermore, constraints (6) ensure that an EP will only be assigned to one ED at most when it departs from a depot. Constraints (7) ensure that an EP can return to a depot at most once within a batch of services. Constraints (2) - (7) altogether ensure that for any arc $a \in A$, an EP can only charge at most one ED at a time. To show this point, we consider that EP(s) charges two different EDs, i and j along the same arc a ($z_{i,a}^s = 1$ and $z_{j,a}^s = 1$), we can derive that there will exist some nodes n and m for which $o_i^{n,s} = 1$ and $o_j^{m,s} = 1$ from constraints (2) - (5). This leads to the contradiction with constraints (6).

4.2. ED and EP energy constraint

We next discuss constraints (8)-(12) to demonstrate how our model ensures the feasible energy inventory of the EDs and the EPs during the service. First of all, the constraints set (8)-(10) ensures the batteries of the EDs are not depleted during the trips. Specifically, e_n^i is used to denote the energy inventory of ED(i) at any node $n \in \mathcal{N}_i \setminus i_0$. It is formulated by three items in constraints (8). The first item of constraints (8) is the energy inventory of ED(i) upon departure. The second item of constraints (8) is the total energy that ED(i) receives before arriving at node n , where $e_{i,a}^+ \left(\sum_{s \in \mathcal{S}} z_{i,a}^s \right)$ indicates the electricity that ED(i) receives along the arc a . The last item of Equation (8) is the total energy that ED(i) consumes before it arrives at node n . Note that the energy reception in the second item of Equation (8) is non-linear. Therefore, to facilitate computation, we introduce auxiliary variables $\gamma_{i,a} = e_{i,a}^+ \left(\sum_{s \in \mathcal{S}} z_{i,a}^s \right)$, $\forall i \in \mathcal{D}, a \in A_i$ and develop Equations (8.1)-(8.4) below to linearize the non-linear term of $e_{i,a}^+ \left(\sum_{s \in \mathcal{S}} z_{i,a}^s \right)$ in constraint (8), where M is a sufficiently big value.

$$\gamma_{i,a} - e_{i,a}^+ \leq 0, \quad \forall i \in \mathcal{D}, a \in A_i \quad (8.1)$$

$$\gamma_{i,a} - M \left(\sum_{s \in \mathcal{S}} z_{i,a}^s \right) \leq 0, \quad \forall i \in \mathcal{D}, a \in A_i \quad (8.2)$$

$$M \left(\sum_{s \in \mathcal{S}} z_{i,a}^s - 1 \right) - \gamma_{i,a} + e_{i,a}^+ \leq 0, \quad \forall i \in \mathcal{D}, a \in A_i \quad (8.3)$$

$$\gamma_{i,a} \geq 0, \quad \forall i \in \mathcal{D}, a \in A_i \quad (8.4)$$

More exactly, Equations (8.1) and (8.3) ensure $\gamma_{i,a} = e_{i,a}^+$ when $\sum_{s \in \mathcal{S}} z_{i,a}^s = 1$. Equations (8.2) and (8.4) ensures $\gamma_{i,a} = 0$ when $\sum_{s \in \mathcal{S}} z_{i,a}^s = 0$. Constraints (9) bound the variable $e_{i,a}^+$ with given maximum energy that ED(i) can receive on arc a (i.e., parameter $\bar{e}_{i,a}^+$). It depends on the travel time to go through the arc and power transfer rate η . Constraints (10) ensure that the battery inventory of the EDs is always above safety inventory e_{-d} and not exceeds battery capacity \bar{e}_i . To be noted, here we model the total energy that an ED receives as a decision variable, which is determined to ensure EDs have enough energy to reach their destinations. However, the model can also fit the scenario in which the EDs requires the level of charge, \hat{e}_i by themselves (i.e., inputs to the model) by introducing a constraint, $\sum_{a \in A_i} \gamma_{i,a} \geq \hat{e}_i$, $\forall i \in \mathcal{D}$.

On the other hand, the routing plan will ensure energy availability so that each EP can return to a depot for recharging. We model the total energy loss of an EP during a trip, E_s , by Equation (11). It includes four items, respectively, counting the energy loss of an EP before, during, and after the charging service in a trip. More precisely, the first item ($\sum \sum o_i^{n,s} e_{s_0 \rightarrow n}^-$) represents the idle energy loss for an EP to reach the first service reception location n from its initial departure location s_0 (i.e., $o_i^{n,s} = 1$). The second item ($\sum \sum \sum v_{ij}^{n,m,s} e_{n \rightarrow m}^-$) is the required energy for an EP to conduct distant switch services over all possibilities. The third item ($\sum \sum z_{i,a}^s e_{i,a}^+ + \sum \sum z_{i,a}^s e_{s,a}^-$) consists of the energy distributed to EDs ($z_{i,a}^s e_{i,a}^+$) and self-consumed ($z_{i,a}^s e_{s,a}^-$) during the services, and the last item ($\sum \sum q_i^{n,s} e_{n \rightarrow p_n}^-$) represents the idle energy loss for an EP returning to the nearest depot p_n from node n . Built upon constraints (11), constraints (12) ensure that the energy inventory of an EP is always above the safety inventory e_{-s} during the service, where e_0^s is the initial energy inventory of an EP. Moreover, we use the similar linearization approach adopted in the constraints set (8.1)-(8.4) to linearize the non-linear term $z_{i,a}^s e_{i,a}^+$ in Equation (11). With additional set of auxiliary variables, $\zeta_{i,a}^s = z_{i,a}^s e_{i,a}^+$, $\forall i \in \mathcal{D}, a \in A_i, s \in \mathcal{S}$, constraints set (11.1) to (11.4) are provided below.

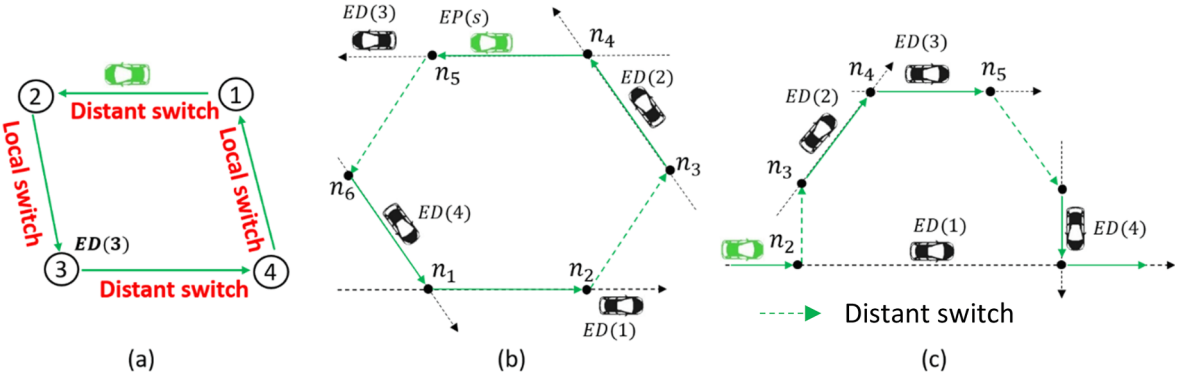


Fig. 3. (a) Example of the subtour with EDs as nodes and local-/distant-switches as links; (b) An illegal subtour example of (a); (c) A legal subtour example of (a).

$$\zeta_{i,a}^s - e_{i,a}^+ \leq 0, \quad \forall i \in \mathcal{D}, a \in A_i, s \in \mathcal{S} \quad (11.1)$$

$$\zeta_{i,a}^s - M\zeta_{i,a}^s \leq 0, \quad \forall i \in \mathcal{D}, a \in A_i, s \in \mathcal{S} \quad (11.2)$$

$$M(\zeta_{i,a}^s - 1) - \zeta_{i,a}^s + e_{i,a}^+ \leq 0, \quad \forall i \in \mathcal{D}, a \in A_i, s \in \mathcal{S} \quad (11.3)$$

$$\zeta_{i,a}^s \geq 0, \quad \forall i \in \mathcal{D}, a \in A_i, s \in \mathcal{S} \quad (11.4)$$

4.3. Subtour elimination constraint

The flow conservation and ED/EP energy constraints rule out the infeasible routes that result in the imbalance flows and energy infeasibility. However, those constraints do not prevent the solution which has an EP to revisit the node and serve the same ED. This study considers a service loop that revisits the same ED as a subtour. Fig. 3(a) shows an example. Specifically, an EP leaves ED(1), conducts a series of local or distant switches to charge several other customers, and eventually, it switches back to serve ED(1) without going back to the depot. Note that this type of subtour is not a route loop on the graph $G(\mathcal{N}, \mathcal{A})$ but a service loop. It further differentiates the subtour issues of the mE2-VRP from the typical VRP models in the literature. More precisely, the subtour of a typical VRP is defined as a tour that revisits the same customer coincident with the network node for developing the VRP model. However, the mE2-VRP is built upon an encounter network, on which EDs are moving toward their destinations. An encounter node of the network does not represent a customer (ED). Accordingly, the mE2-VRP allows an EP service tour to revisit the same encounter node for serving different EDs or revisit the same ED at different encounter nodes. We only exclude the situation where an EP revisiting the same ED at the same encounter node since it conflicts with the temporal-spatial feasibility given the ED is moving toward its destination in our problem. Therefore, the subtours in the mE2-VRP can be either illegal or legal shown in Fig. 3.

Fig. 3(b) shows an illegal subtour, where EP(s) serves EDs from (1) to (4) and then revisit ED(1) at the same node n_1 ; this service loop is temporally infeasible. More exactly, EP(s) starts the route by serving ED(1) from nodes n_1 to n_2 . At node n_2 , it travels to node n_3 and serves ED(2) (i.e., an distant switch). After that, EP(s) switches the service to charge ED(3) and then ED(4). Last, the EP(s) arrives at node n_1 and switches the service back to ED(1) at n_1 . This subtour makes EP(s) visit ED(1) at the same node n_1 twice but at different time stamps, which is temporally impossible given ED(1) is always on the move toward its destination during this period. Thus, this is an illegal subtour. Fig. 3(c) shows an illegal subtour. It starts with charging the ED(1) and moving toward the node n_1 and then (local/distant) switches to a series of EDs(2 to 4) and finally switch back to charge ED(1) at n_2 . This subtour forms a service loop by revisiting ED(1) at node n_1 and n_2 respectively. Given that partial charging is allowed, this revisit is permitted and then the subtour is legal.

Conventional subtour elimination constraints, e.g., the MTZ constraints (Miller et al., 1960), track the visiting orders of customers (they are also the nodes in the network) and remove all the tours that revisit the same customers. Therefore, using existing subtour elimination constraints will remove both the illegal tours such as Fig. 3(b) and legal tours such as Fig. 3(c). Thus, they do not adapt to this study. We develop new subtour elimination constraints in (13) and (14). They trace the visiting time of an EP at each encounter node (not at each ED) and allow a revisiting only if it is carried out by a temporal feasible (distant or local) switch. Therefore, our subtour elimination constraints only eliminate the illegal subtours but keep the legal ones. We prove the correctness of our subtour elimination constraints by Theorem 1. To facilitate the development of the proof, we categorize the illegal subtours into three types: the subtour (1) purely formed by distant switches, (2) purely formed by local switches, and (3) mixed with distant and local switches. Then, we prove that constraints (13)(14) can eliminate these three types of illegal subtours (Lemma 1 – 3).

Lemma 1. *For any $ED(i)$, a trip satisfying (13) and (14) eliminates the illegal subtours that are only formed by distant switch from/back to $ED(i)$.*

Proof. We prove Lemma 1 contradiction. Let n be the number of EDs involved in the subtour. The proof starts with the case involving two EDs (i.e., $n = 2$), and then extends to a general case with $n \geq 3$. We consider that there exists an illegal subtour purely formed by distant switches as $n = 2$, and this subtour satisfies (13) and (14). For example, $ED(i_1)$ and $ED(i_2)$ in Fig. 4(a), in which both

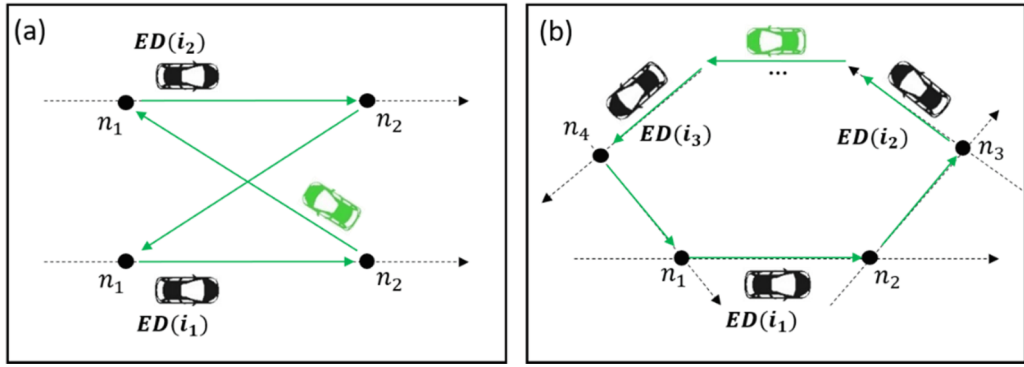


Fig. 4. Illegal subtours formed by the distant switches only. (a) $n = 2$ and (b) $n \geq 3$.

$ED(i_1)$ and $ED(i_2)$ travel from node n_1 to node n_2 . Without loss of generality, we assume an EP serves $ED(i_1)$ as they move from node n_1 to n_2 and conducts distant switch to serve $ED(i_2)$ at node n_1 (i.e., $v_{i_1,i_2}^{n_2,n_1,s} = 1$). Then, the EP serves $ED(i_2)$ until it arrives at node n_2 , from which the EP moves back to node n_1 and revisit $ED(i_1)$ (i.e., does a distant switch from n_2 to n_1 (i.e., $v_{i_2,i_1}^{n_2,n_1,s} = 1$)). Clearly, this subtour is illegal as it makes the EP revisit $ED(i_1)$ at node n_1 at different time stamps. We show the conflict resulting from the illegal subtour as follows. Given constraint (14) is satisfied with $v_{i_1,i_2}^{n_2,n_1,s} = v_{i_2,i_1}^{n_2,n_1,s} = 1$, we have (16) and (17).

$$t_{i_2}^{n_1} - t_{i_1}^{n_2} - t_{n_1 \rightarrow n_2} \geq 0 \quad (16)$$

$$t_{i_1}^{n_1} - t_{i_2}^{n_2} - t_{n_2 \rightarrow n_1} \geq 0 \quad (17)$$

Adding (16) and (17) together and restructuring the result, we have

$$-2t_{n_2 \rightarrow n_1} \geq (t_{i_2}^{n_2} - t_{i_1}^{n_1}) + (t_{i_2}^{n_2} - t_{i_2}^{n_1}) > 0 \quad (18)$$

Equation (18) indicates that $t_{n_2 \rightarrow n_1} < 0$, which contradicts with the fact $t_{n_2 \rightarrow n_1} > 0$. Therefore, such subtour does not exist.

When the case with $n \geq 3$ (see Fig. 4(b) for an example), we assume an EP serves $ED(i_1)$ from node n_1 to n_2 and conducts distant switch to serve $ED(i_2)$ ($v_{i_1,i_2}^{n_2,n_3,s} = 1$). Then, the EP continues to serve several other EDs by multiple distant switches and finally revisit $ED(i_1)$ at node n_1 after it leaves $ED(i_3)$ ($v_{i_3,i_1}^{n_4,n_1,s} = 1$) from node n_4 . Focusing on the feasibility of the first and last distant switches associated with $ED(i_1)$, we have (19)(20) below given constraint (14) is satisfied with $v_{i_1,i_2}^{n_2,n_3,s} = v_{i_3,i_1}^{n_4,n_1,s} = 1$.

$$t_{i_2}^{n_3} - t_{i_1}^{n_2} - t_{n_2 \rightarrow n_3} \geq 0 \quad (19)$$

$$t_{i_1}^{n_1} - t_{i_3}^{n_4} - t_{n_4 \rightarrow n_1} \geq 0 \quad (20)$$

Adding (19) and (20) together and restructuring the result, we have (21) below.

$$-t_{n_4 \rightarrow n_1} - t_{n_2 \rightarrow n_3} \geq (t_{i_2}^{n_2} - t_{i_1}^{n_1}) + (t_{i_3}^{n_4} - t_{i_2}^{n_3}) > 0 \quad (21)$$

(21) indicates that $t_{n_4 \rightarrow n_1} + t_{n_2 \rightarrow n_3} < 0$, which contradicts with $t_{n_2 \rightarrow n_3} > 0, t_{n_4 \rightarrow n_1} > 0$. Therefore, the subtour does not exist. We thus complete the proof.

Lemma 2. For any $ED(i)$, a trip satisfying (13) and (14) eliminates subtours that are only formed by local switch from/back to $ED(i)$.

Proof. The procedure to prove this lemma is similar to the proof of Lemma 1. We leave it in Appendix E.

Lemma 3. For any $ED(i)$, a trip satisfying (13) and (14) eliminates subtours that are formed by distant switch from/back to and local switch back to/from $ED(i)$.

Proof. The procedure to prove this lemma is similar to the proof of Lemma 1. We leave it in Appendix E.

Theorem 1. Constraints (13)(14) are valid subtour elimination constraints for the mE2-VRP model.

Proof. Theorem 1 is immediately proved by Lemma 1–3.

5. Clustering-Aided decomposition and merging

The mE2-VRP is a mixed-integer program subject to many constraints, which is an NP-hard problem in general. Moreover, the mE2-VRP considers the on-the-move electricity delivery and allows an EP to revisit the same ED multiple times. These unique features introduce extra complexity to the mE2-VRP. Finding the optimal solution of the mE2-VRP may be a computationally impractical task.

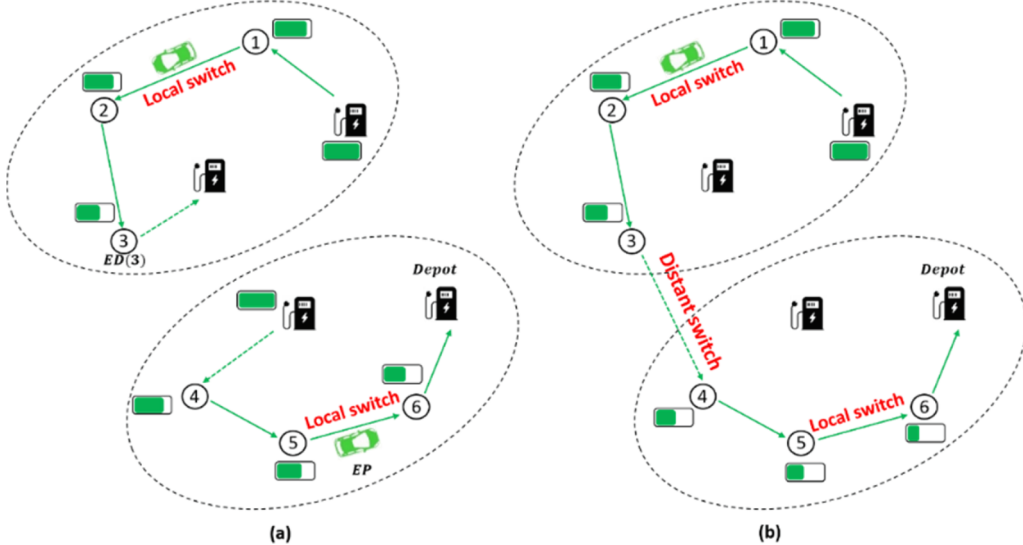


Fig. 5. Schematic representation of the c-DM algorithm.

This study, therefore, focuses on efficiently searching for a good-quality solution to satisfy the timely service requirement of CaaS⁺. Accordingly, we design a clustering-aided decomposition and merging (c-DM) algorithm as a heuristic approach. The development of this algorithm takes advantage of the special features of this problem. The main idea of the c-DM algorithm is introduced as follows.

First of all, it is noticed that the computation complexity of the mE2-VRP increases significantly as more EDs are involved in the problem. This is because those EDs will introduce more nodes and arcs to the graph $G(\mathcal{N}, \mathcal{A})$ and complicate its topology. As a result, it makes the feasible trips of EPs (feasible solution) enormous. However, we also can observe that some EDs, constrained by their trip plans, have a high potential to form a coalition served by one EP, but others not, which can be treated separately. By understanding this feature in depths, the c-DM algorithm first strategically splits all EDs into multiple clusters according to their coalition potential. It enables us to decompose the master problem (i.e., mE2-VRP) into a number of subproblems (i.e., sub-mE2-VRPs). Each subproblem has a small instance size and can be efficiently solved by existing commercial solvers such as Gurobi. Next, we solve each sub-mE2-VRP simultaneously by parallel computing to obtain the seed tours, all of which together form the first feasible solution of the master mE2-VRP. Fig. 5 (a) shows an example. Last, this study further improves the initial feasible solution by strategically merging the seed tours over all clusters. It will help reduce the size of the EP fleet and represents a better solution for the master mE2-VRP (see the illustration of the idea in Fig. 5 (b)). In summary, the c-DM algorithm includes three key steps as follows.

Step 1: Form the ED clusters according to the coalition potential and decompose the master problem into the sub-mE2-VRPs.

Step 2: Parallelly solve each sub-mE2-VRP and generate seed tours.

Step 3: Merge seed tours to explore a better solution.

There are several critical technical issues in each of the three steps above, which will affect the performance of the c-DM algorithm significantly. Mainly, to ensure a good initial solution formed by the seed tours, the ED clusters should be strategically formed so that we can minimize the compromise of the global optimality resulting from the decomposition. Moreover, the c-DM algorithm requires careful efforts to solve the subproblems and develop an appropriate merging algorithm to secure the feasibility and efficiency of the improved solution. We discuss our approaches to address these technical difficulties in detail in the following sections.

5.1. Forming ED clusters according to coalition potential

We first discuss how to form the ED clusters so that they can facilitate the solution exploration as much as possible. It is noticed that distant switches are expensive since each distant switch causes extra idle energy and time loss. Therefore, an optimal solution prefers local switches rather than distant switches. Following this thought, we recognized that the EDs tend to have a high coalition potential (using the same EP for their services) if there are more local switch opportunities between them. If we cluster the EDs with high coalition potential and then explore the seed tours in each cluster to form the initial solution, this decomposition is likely to lead to a good feasible solution without over sacrificing global optimality. Invoked by these observations, this study first develops a quantitative index to measure the coalition potential among EDs by factoring in the possibility of the local switch occurring between two EDs according to their trip plans. Built upon that, we develop a clustering algorithm to form the ED clusters. More precisely, the clustering algorithm seeks to put two EDs in one cluster if their trips present a high coalition potential; otherwise, they will be separated into different clusters. Note that we temporally ignore the limit of the energy inventory as we form the ED clusters.

Our clustering algorithm consists of two parts. (1) Measure the coalition potential between any pair of the EDs considering their routes and trip schedules. (2) Forming the ED clusters with high coalition potential among the EDs in each cluster.

To quantify the coalition potential, we consider two EDs such as i and j , both of which will pass node n in $G(\mathcal{N}, \mathcal{A})$. If ED(i) under the

service of an EP arrives at node n is earlier than $\text{ED}(j)$ does (i.e., $t_n^i - t_n^j \geq 0$), then potentially the EP can locally switch from $\text{ED}(i)$ to serve $\text{ED}(j)$ at node n . All such $\text{ED}(j)$ form the potential coalition for $\text{ED}(i)$ at node n , which is labeled as $J_{i,n}$. The size of the potential coalition can help us to measure the opportunities that local switches will occur between a given ED and all other EDs. An ED with a larger potential coalition will have more opportunities to enable an EP on duty with it to do a local switch and continue to serve the other EDs at a node. Accordingly, we formally define the potential coalition of $\text{ED}(i)$ at node n in (22).

$$J_{i,n} = \{\text{ED}(j) | t_n^i - t_n^j \geq 0, j \in D_n, j \neq i\}, i \in \mathcal{D}, n \in \mathcal{N}_i \setminus i_0; J = \{J_{i,n}\}_{\{i \in \mathcal{D}, n \in \mathcal{N}_i \setminus i_0\}} \quad (22)$$

Recall that $t_n^i = \tilde{t}_0^i + t_{i_0 \rightarrow n} + \tau_i$, $t_n^j = \tilde{t}_0^j + t_{j_0 \rightarrow n} + \tau_j$ in (15), and τ_i and τ_j are continuous variable respectively representing the waiting time of $\text{ED}(i)$ and $\text{ED}(j)$, $0 \leq \tau_i \leq \bar{\tau}_i, 0 \leq \tau_j \leq \bar{\tau}_j$. Given τ_i and τ_j are unknown decision variables in the mE2-VRPs mathematical model, we are not able to directly apply set $J_{i,n}$ in the development of the clustering algorithm. Thus, we consider another equivalent set $\bar{J}_{i,n}$ defined by (23) which explicitly formulates the potential coalition of an ED at a node, using known parameters \tilde{t}_0^i , \tilde{t}_0^j , $t_{i_0 \rightarrow n}$ and $t_{j_0 \rightarrow n}$. Lemma 4 proves the equivalence of $\bar{J}_{i,n}$ and $J_{i,n}$ as well as J and \bar{J} .

$$\bar{J}_{i,n} = \{\text{ED}(j) | (\tilde{t}_0^j + t_{j_0 \rightarrow n}) - (\tilde{t}_0^i + t_{i_0 \rightarrow n}) \geq -\bar{\tau}_j, j \in D_n, j \neq i\}, i \in \mathcal{D}, n \in \mathcal{N}_i \setminus i_0; \quad (23)$$

$$\bar{J} = \{\bar{J}_{i,n}\}_{\{i \in \mathcal{D}, n \in \mathcal{N}_i \setminus i_0\}}$$

Lemma 4. *The two sets $\bar{J} = \{\bar{J}_{i,n}\}_{\{i \in \mathcal{D}, n \in \mathcal{N}_i \setminus i_0\}}$ and $J = \{J_{i,n}\}_{\{i \in \mathcal{D}, n \in \mathcal{N}_i \setminus i_0\}}$ are equivalent.*

Proof. We first prove $J \subseteq \bar{J}$. To do it, our proof shows that any $\text{ED}(j)$ in the set of $J_{i,n}$ belongs to $\bar{J}_{i,n}$ too, i.e., $J_{i,n} \subseteq \bar{J}_{i,n}, \forall i \in \mathcal{D}, n \in \mathcal{N}_i \setminus i_0$. According to (22) and (15), we have (24)-(26) for any $\text{ED}(j) \in J_{i,n}$.

$$t_n^i - t_n^j \geq 0 \Leftrightarrow (\tilde{t}_0^j + t_{j_0 \rightarrow n} + \tau_j) - (\tilde{t}_0^i + t_{i_0 \rightarrow n} + \tau_i) \geq 0 \quad (24)$$

$$0 \leq \tau_i \leq \bar{\tau}_i \quad (25)$$

$$0 \leq \tau_j \leq \bar{\tau}_j \quad (26)$$

According to (25) and (26), we restructure (24) to get (27) below for $\text{ED}(j) \in J_{i,n}$.

$$(\tilde{t}_0^j + t_{j_0 \rightarrow n}) - (\tilde{t}_0^i + t_{i_0 \rightarrow n}) \geq \tau_i - \tau_j \geq -\bar{\tau}_j \quad (27)$$

Then, (23) and (27) together indicate that $\text{ED}(j) \in \bar{J}_{i,n}$ for any $\text{ED}(j) \in J_{i,n}$. Therefore, we have the conclusion in (28).

$$J_{i,n} \subseteq \bar{J}_{i,n}, \forall i \in \mathcal{D}, n \in \mathcal{N}_i \setminus i_0 \Leftrightarrow J \subseteq \bar{J} \quad (28)$$

We next prove that $\bar{J} \subseteq J$ by showing that any $\text{ED}(j)$ in the set of $\bar{J}_{i,n}$ belongs to $J_{i,n}$ too, i.e., $\bar{J}_{i,n} \subseteq J_{i,n}, \forall i \in \mathcal{D}, n \in \mathcal{N}_i \setminus i_0$. To do that, we denote a set for all possible waiting time tuples (τ_i, τ_j) for $\text{ED}(j)$ in $J_{i,n}$ as

$$\Omega_{i,j}^n = \left\{ (\tau_i, \tau_j) | (\tilde{t}_0^j + t_{j_0 \rightarrow n} + \tau_j) - (\tilde{t}_0^i + t_{i_0 \rightarrow n} + \tau_i) \geq 0, 0 \leq \tau_i \leq \bar{\tau}_i, 0 \leq \tau_j \leq \bar{\tau}_j \right\}, i \in \mathcal{D}, n \in \mathcal{N}_i \setminus i_0, j \in D_n, j \neq i$$

Clearly, if we can find a pair of waiting time (τ_i, τ_j) for $\text{ED}(i)$ and $\text{ED}(j)$ in $\Omega_{i,j}^n$, then $\text{ED}(j)$ is in the set of $J_{i,n}$. Considering any $j \in \bar{J}_{i,n}$, we have (29) according to (23).

$$(\tilde{t}_0^j + t_{j_0 \rightarrow n} + \bar{\tau}_j) - (\tilde{t}_0^i + t_{i_0 \rightarrow n}) \geq 0 \quad (29)$$

(29) indicates that there exists a waiting time tuple: $\tau_j = \bar{\tau}_j$ and $\tau_i = 0$ such that $(\tau_j, \tau_i) \in \Omega_{i,j}^n$. Therefore, we conclude that any $j \in \bar{J}_{i,n}$ satisfies $j \in J_{i,n}$, and thus we have the result in (30).

$$\bar{J}_{i,n} \subseteq J_{i,n}, \forall i \in \mathcal{D}, n \in \mathcal{N}_i \setminus i_0 \Leftrightarrow \bar{J} \subseteq J \quad (30)$$

Combining the results in (28) and (30), we conclude Lemma 4 #.

The set $\bar{J}_{i,n}$ help us understand the chance that a local switch may occur between $\text{ED}(i)$ and all other EDs at a single node n . It is not sufficient for the design of the clustering algorithm since it still cannot capture the opportunities for an EP to perform local switches between a pair of EDs. To solve this issue, we develop a coalition potential matrix (CP-matrix), Equation (31), based upon the set \bar{J} , which measures the coalition potential between a pair of EDs such as i and j by the number of potential local switches from $\text{ED}(i)$ to $\text{ED}(j)$ along the route of $\text{ED}(i)$.

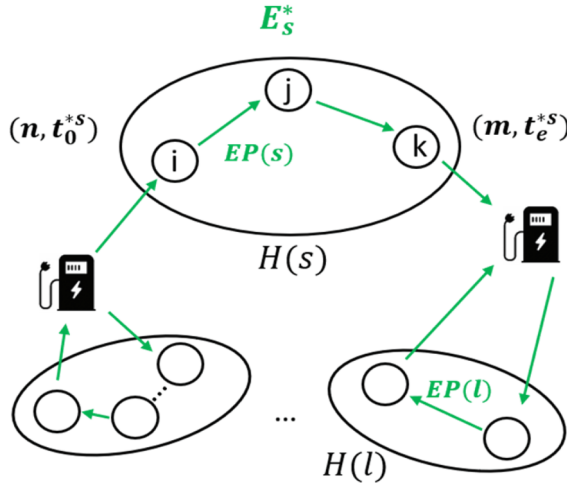


Fig. 6. An example of seed tours.

$$p(i,j) = \begin{cases} \sum_{n \in \mathcal{N}_i \setminus i_0} \mathbb{I}\{j \in J_{i,n}\}, \forall i, j \in D, i \neq j \\ 0, i = j \end{cases} \quad \text{and } P = [p(i,j)]_{i,j \in D} \quad (31)$$

where $\mathbb{I}\{j \in J_{i,n}\}$ is an indicator function, takes value 1 when $j \in J_{i,n}$.

Last, built upon the coalition potential matrix, we design the clustering algorithm to form ED clusters. Mainly, the clustering algorithm starts with the ED pair that has the largest coalition potential and puts them in one cluster, then iteratively clusters the next promising ED in the same cluster until no more ED can be locally switched to. Appendix C presents and explains the steps of the pseudocode of our clustering algorithm.

5.2. Generating seed tours to form a feasible solution

We next discuss the second step of the c-DM algorithm, which seeks to solve the sub-mE2-VRP for each cluster efficiently. Our experiments noticed that each subproblem may still involve many EDs (such as greater than 100 EDs) as we implement CaaS⁺ in a large network. This is because the clustering algorithm is an unsupervised learning algorithm and cannot pre-determine the size of each ED cluster. As a result, the corresponding sub-mE2-VRP may still have many variables and constraints and is difficult to be solved within planning interval length T . To address this challenge, the study develops the scheme shown in (32). It disables distant switches for each cluster c to sustain the computation efficiency and solution quality by leveraging two critical features of the problem. First of all, we observed that distant switch services contribute most to the model complexity since each of them introduces more variables and constraints than a local switch does in the mathematical model. Next, considering the clusters are formed with particular interest to promote local switch services in each cluster, we have a strong reason to believe that an optimal solution of each subproblem will involve more local switches than distant switch services. Thanks to these merits of the ED clusters, disabling distant switches in a subproblem will benefit the computation load without over sacrificing the solution quality for solving the sub-mE2-VRP. In the meantime, the complexity of the sub-mE2-VRP(c) is significantly reduced and these subproblems can be quickly solved (find seed tours) by commercial solvers using parallel computation. It is worth mentioning that even though we can disable the distant switch services in the master mE2-VRP, it is still a large-scale mixed integer programming and is very hard to be solved. In addition, without the merits of the clustering algorithm, this simplification will comprise the optimality significantly.

$$\text{sub-mE2-VRP}(c) : \left\{ \min F(O), s.t. v_{ij}^{n,m,s} = 0, \forall v \in V; s \in \mathcal{S}, i \in \mathcal{D}; (2) \sim (13) \right\} \quad (32)$$

Putting all the seed tours together we can quickly obtain the initial feasible solution of the mE2-VRP. Mathematically, we denote $\mathcal{S}_0 \subseteq \mathcal{S}$ as the set of the EPs that are dispatched in the initial feasible solution. Then, each EP(s) in \mathcal{S}_0 is associated with a seed tour $H(s)$, $s \in \mathcal{S}_0$ (see Fig. 6). Accordingly, Equation (33) includes all necessary information of a seed tour $H(s)$ required for merging which will be discussed later, where n and t_0^{*s} represents the locations and the time that EP(s) start the service in the seed tour. Here, we use (*) to represent the optimal solution of sub-mE2-VRP. Similarly, m and t_e^{*s} represents the locations and the time that EP(s) completes the service with the last ED in the seed tour.

$$H(s) = (n, t_0^{*s}, m, t_e^{*s}, E_s^*) \quad (33)$$

Last, E_s^* represents the total energy losses of EP(s) during this seed tour. Note that E_s^* excludes the idle energy losses from a depot to the first ED, and from the last ED to the depot.

Now consider any EP(s) in \mathcal{S}_0 , we denote $\mathcal{D}_s^* \subseteq \mathcal{D}$ as the set of the EDs served by the EP(s), e.g., $\mathcal{D}_s^* = \{i, j, k\}$ in an example of

Fig. 6. Specifically, we use $s(n)$ to represent the n -th ED that EP(s) serves in the seed tour, e.g., $s(1) = i$, $s(2) = j$, and the last ED that EP(s) serves is denoted as $s(-1)$, e.g., $s(-1) = k$. With these notations, we introduce how to merge the seed tours and improve the initial feasible solution in the next section.

5.3. Merging seed tours to refine the feasible solution

The initial feasible solution obtained in Step 2 excludes any distant switch service between the EP trips formed in individual clusters. Given the mE2-VRP seeks to fulfill the service requests with a minimum fleet size, this study next wants to further improve this feasible solution by merging those seed tours by adding back the distant switches. To present our main idea, let's consider two seed tours, $H(s) = (n_1, t_0^{*s}, n_2, t_e^{*s}, E_s^*)$ and $H(l) = (m_1, t_0^{*l}, m_2, t_e^{*l}, E_l^*)$, $s, l \in \mathcal{S}_0$. The merging algorithm seeks to have an EP serve the EDs in the seed tour $H(s)$ first and then $H(l)$ without violating the energy feasibility (Rule 1) and delay tolerance (Rule 2). Each successful merging will reduce the fleet size of the initial feasible solution by one. More precisely, we would like to merge two seed tours to one if an EP has enough energy to fulfill the service requests of the EDs in the other seed tour such as $H(l)$ after it finishes with the seed tour on duty such as $H(s)$. Clearly, each merging introduces one more distant switch (and also delay), by which the EP travels from the tail of $H(s)$ to the head of $H(l)$. Therefore, a successful switch needs to also satisfy the delay tolerance required by the EDs in the second seed tour of $H(l)$. Following this idea, we developed the merging algorithm according to the two merging rules in (34) and (35).

$$\text{Rule1} : e_0^s - \left(e_{s_0, n_1}^- + E_s^* \right) - e_{n_2, m_1}^- - \left(E_l^* + e_{m_2, p_{m_2}}^- \right) \geq e_{-s}$$
 (34)

$$\text{Rule2} : (t_e^{*s} + t_{n_2 \rightarrow m_1}) - t_0^{*l} \leq \min \{ \bar{\tau}_i - \tau_i^*, \forall i \in \mathcal{D}_l^* \}$$
 (35)

Rule 1 ensures that EP(s) has enough energy to fulfill energy requests of the EDs in $H(l)$. Mainly, the first item is the initial energy inventory of EP(s), the second and fourth item are the energy losses associated with the seed tours $H(s)$ and $H(l)$, respectively. The third item is the energy required to do the distant switch (merging). After serving all the EDs in both seed tours, the EP should have enough energy left to go back to the depot. **Rule 2** guarantees that EP(s) can timely meet every EDs in the second seed tour without violating their waiting tolerance. The left-hand-side of Rule 2 is the extra delay resulting from the merging, which involves the difference of two items. The first one is the time that EP(s) can start serving the head of $H(l)$ if these two seed tours, $H(s)$ and $H(l)$ are merged, and the second item is the time that the head of $H(l)$ is served by EP(l) in the pre-merging solution. The right-hand-side of Rule 2 is the upper bound of the extra delay imposed by the EDs in $H(l)$. Each ED(i) in $H(l)$ has a tolerable delay $\bar{\tau}_i$ and an actual delay, τ_i^* in the pre-merging solution. Therefore, $\bar{\tau}_i - \tau_i^*$ is the extra delay that ED(i) can tolerate if two seed tours are merged. The minimum of these extra delays bounds the extra delay from merging so that the waiting tolerance of all the EDs in $H(l)$ will not be violated.

The algorithm is interested in merging as many as possible seed tours to one EP trip so that we can minimize the size of the EP fleet. To achieve this, we notice that the departure time after an EP finishes with the last ED in a merged tour is critical. To facilitate our discussion, we denote a merged tour in the example above as $\bar{H}(s-l)$ and this departure time from the tour as t_e^{*-l} . We found that an EP leaving the $\bar{H}(s-l)$ earlier will have more opportunities to accommodate another seed tour following the tour of $\bar{H}(s-l)$ in one trip. Consequently, our merging algorithm gives high priority to merge a pair of seed tours which leads to a smaller value of t_e^{*-l} . Appendix D provides the pseudocode of the merging algorithm. Here, we briefly discuss the main steps of our merging algorithm. We first find all feasible seed tours for merging according to Rule 1 and Rule 2 and rank their priority. Following that, we select the best feasible seed tours to merge according to their priority. Last, considering the merged tour as a new tour, repeat the first two steps until no more feasible merging pair can be found.

Note that our current merging algorithm (objective saving is one for each merging) is designed based on the objective to minimize the fleet size. If the objective function is extended to minimize total travel costs or idle energy losses, the merging algorithm can be updated by modifying the calculation of objective savings accordingly.

5.4. The feasibility of the c-DM algorithm

This section discusses if the c-DM algorithm can guarantee a feasible solution to the mE2-VRP. Clearly, the initial solution formed by gathering the seed tours from solving the subproblems is feasible to the mE2-VRP by putting all distant switch variables equal to zeros (i.e., making constraint (14) always correct). Our doubt is raised by the merging process which adds back distant switches according to constraints (34) and (35). More precisely, constraint (34) that is used to ensure the energy feasibility in the c-DM algorithm is different from the energy inventory constraint (12) in the mE2-VRP. Similarly, constraint (35) used to secure the delay tolerance in the c-DM algorithm is also different from constraints (13) and (14), which ensure the feasible local and distant switches according to the EDs' delay tolerance. In view of these issues, this section proves that a solution obtained from c-DM algorithm satisfying constraints (34) and (35) will also satisfy constraints (12), (13), and (14), respectively. In this way, we can guarantee that the c-DM algorithm finds a good feasible solution to the mE2-VRP. Lemma 5 below summarizes this thought.

Lemma 5. An EP tour obtained by merging the seed tours of the c-DM algorithm according to constraints (34) and (35) will satisfy constraints (12), (13), and (14) in the mE2-VRP.

Proof. First, the seed tours of the c-DM algorithm are obtained by solving the sub-mE2-VRPs. Therefore, they satisfy constraints (12), (13), and (14) in the mE2-VRP. Next, we further prove that merging these seed tours according to (34) and (35) won't violate

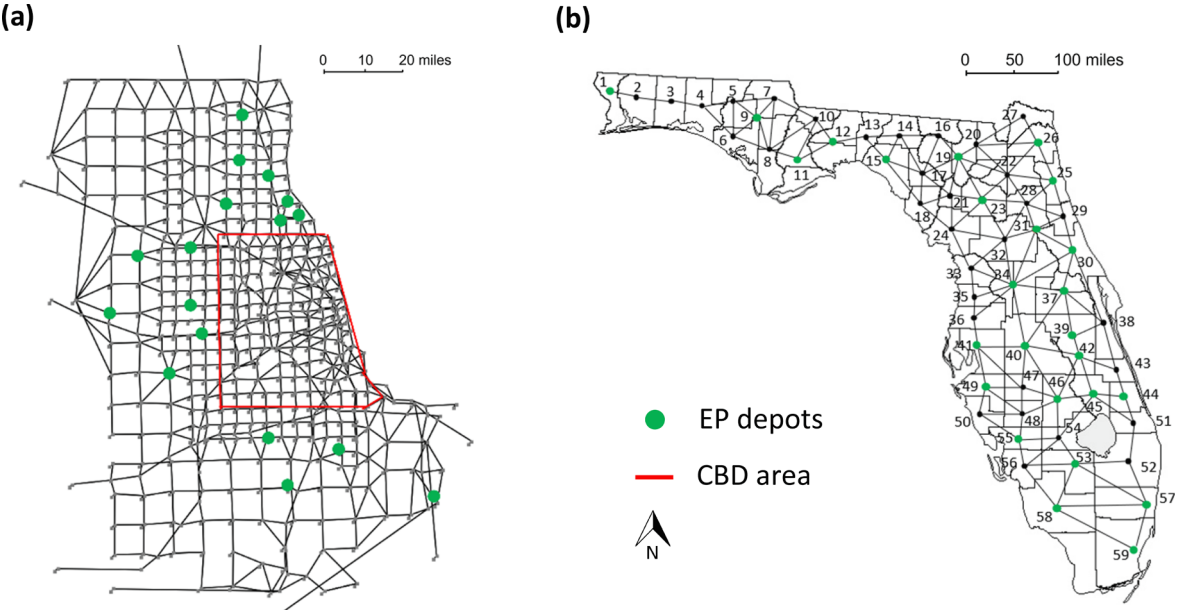


Fig. 7. Test network. (a) Chicago sketch network and the EP depots (green nodes), (b) Florida network and EP depots (green nodes). (For interpretation of the references to colour in this figure legend, the reader is referred to the web version of this article.)

constraints (12), (13), and (14).

We first prove that the EP tour obtained satisfying constraint (34) won't violate constraint (12). Clearly, by taking $E_s = e_{s_0 \rightarrow n_1}^- + E_s^* + e_{n_2 \rightarrow m_1}^- + E_l^* + e_{m_2 \rightarrow p_{m_2}}^-$ (the left side of (34)), constraint (34) indicates that $e_0^s - E_s \geq e_{-s}$, which satisfies constraint (12).

We next prove a tour that satisfies constraint (35) also satisfies constraints (14). To conduct this proof, we consider two seed tours, such as $H(s) = (n_1, t_0^{*s}, n_2, t_e^{*s}, E_s^*)$ and $H(l) = (m_1, t_0^{*l}, m_2, t_e^{*l}, E_l^*)$. The c-DM algorithm merges them according to the constraint (35). We denote the last ED in tour $H(s)$ by ED(i) and the first ED in $H(l)$ by ED(j) (i.e., $s(-1) = i, l(0) = j$). They are respectively associated with the waiting time $\tau_i^* \in [0, \bar{\tau}_i]$ and $\tau_j^* \in [0, \bar{\tau}_j]$. The proof first shows that the distant switch from ED(i) to ED(j) (i.e., $v_{i,j}^{n_2, m_1, s} = 1$) satisfies constraint (14). Combining with (15), this is equivalent to prove (36) holds. Namely, there exists feasible waiting delays satisfying the delay requests of ED(i) in $H(s)$ and ED(j) in $H(l)$ such that ED(j) can receive timely service when EP(s) conduct a distant switch from ED(i) to ED(j).

$$\exists \tau_i \in [0, \bar{\tau}_i], \tau_j \in [0, \bar{\tau}_j], s.t \left(\vec{t}_0^i + t_{j_0 \rightarrow m_1} + \tau_i \right) - \left(\vec{t}_0^i + t_{i_0 \rightarrow n_2} + \tau_j \right) - t_{n_2, m_1} \geq 0 \quad (36)$$

To prove the correctness of (36), we consider (35) is satisfied as we merge $H(s)$ and $H(l)$. Given $t_e^{*s} = t_{n_2}^i$ and $t_0^{*l} = t_{m_1}^j$, we plug (15) into (35), and obtain (37).

$$\left(\vec{t}_0^i + t_{j_0 \rightarrow m_1} + \tau_j^* \right) - \left(\vec{t}_0^i + t_{i_0 \rightarrow n_2} + \tau_i^* \right) - t_{n_2, m_1} + \min \{ \bar{\tau}_i - \tau_i^*, \forall i \in \mathcal{D}_l^* \} \geq 0 \quad (37)$$

Now, we can take $\tau_i = \tau_i^* \in [0, \bar{\tau}_i]$, and $\tau_j = \tau_j^* + \min \{ \bar{\tau}_i - \tau_i^*, \forall i \in \mathcal{D}_l^* \} \leq \tau_j^* + \bar{\tau}_j - \tau_j^* = \bar{\tau}_j$ and make (36) hold. Therefore, the merging satisfying (35) won't violate the constraint (14).

Last, we prove a tour that satisfies constraint (35) will make constraints (13) hold too. Clearly, the merging algorithm won't affect the trip plan of the first seed tour such as $H(s)$ in our example. And then all the local switches in $H(s)$ satisfy constraint (13). However, we need to show that the merging can also make the local switches in the second seed tour such as $H(l)$ satisfy constraint (13). Here, we only prove that the first local switch in the seed tour $H(l)$ is feasible. Follow the same logic, the feasibility of other local switches in the $H(l)$ can be easily proved.

We denote the first and the second EDs in the seed tour $H(l)$ by ED(j) and ED(k). The EP(s) conducts a local switch (the first local switch in $H(l)$) at node c from the ED(j) to the ED(k), i.e., $u_{j,k}^{c,s} = 1$. We show this local switch is feasible to constraint (13). Combining with (15), this is equivalent to prove (38) holds. Namely, there exist feasible waiting delays satisfying the delay requests of ED(j) and ED(k) in $H(l)$, such that when two seed tours merge, ED(k) can be timely served by EP(s).

$$\exists \tau_j \in [0, \bar{\tau}_j], \tau_k \in [0, \bar{\tau}_k], s.t \left(\vec{t}_0^k + t_{k_0 \rightarrow m_3} + \tau_k \right) - \left(\vec{t}_0^k + t_{j_0 \rightarrow m_3} + \tau_j \right) \geq 0 \quad (38)$$

We have known that the initial solutions τ_k^* and τ_j^* satisfy constraint (13). By (15), constraint (13) is equivalent to (39).

Table 2

Computation performance of c-DM algorithm under the default setting.

Instance size	Gurobi			c-DM		Service rate
	Solution (1 h)	Solution (2 h)	Opt gap (%)	Solution	Solution time/s	
60	15.6	14.5	0	14.5	5.66	4.14
70	21.3	16.4	0	16.4	6.03	4.27
80	20.9	18.3	5.4	20.3	6.24	3.94
90	23.2	20.9	15.3	21.5	6.98	4.18
100	27.3	23.1	11.3	23.8	7.43	4.20
120	—	—	—	24.0	8.34	5.00
140	—	—	—	24.9	9.56	5.62
200	—	—	—	31.6	13.82	6.33
300	—	—	—	43.6	17.33	6.88
600	—	—	—	85.9	30.90	6.98
1,200	—	—	—	189.6	54.92	6.33
2,000	—	—	—	294.3	110.74	6.79
4,000	—	—	—	579.4	204.34	6.90
6,000	—	—	—	962.5	379.65	6.23
8,000	—	—	—	1,234.2	553.33	6.48
10,000	—	—	—	1,533.3	684.56	6.52

$$t_{m_3}^k - t_{m_3}^j = \left(\tilde{t}_0^k + t_{k_0 \rightarrow m_3} + \tau_k^* \right) - \left(\tilde{t}_0^j + t_{j_0 \rightarrow m_3} + \tau_j^* \right) \geq 0 \quad (39)$$

Now let's take $\tau_j = \tau_j^* + \min\{\bar{\tau}_i - \tau_i^*, \forall i \in \mathcal{D}_l^*\} \leq \bar{\tau}_j$ and $\tau_k = \tau_k^* + \min\{\bar{\tau}_i - \tau_i^*, \forall i \in \mathcal{D}_l^*\} \leq \tau_k^* + \bar{\tau}_k - \tau_k^* = \bar{\tau}_k$. The constraint in (38) becomes $\left(\tilde{t}_0^k + t_{k_0 \rightarrow m_3} + \tau_k^* \right) - \left(\tilde{t}_0^j + t_{j_0 \rightarrow m_3} + \tau_j^* \right) \geq 0$, which is satisfied according to (39). Therefore, there exists $\tau_j \in [0, \bar{\tau}_j]$, $\tau_k \in [0, \bar{\tau}_k]$, such that (38) holds. Now, we can conclude that the local switches after merging are still feasible to constraint (13). Wrapping up all conclusions above, we complete this proof. It also indicates that the merging will not introduce infeasibility.

Theorem 2. *The c-DM algorithm finds a feasible solution to the mE2-VRP.*

Proof. First, the initial solution obtained from the c-DM algorithm is a collection of the solutions of the sub-mE2-VRPs defined by (32), whose constraints are subject to the mE2-VRP. Therefore, this initial solution is feasible to the mE2-VRP. Then, Lemma 5 proves that the merging instrument for involving the distant switches to improve the quality of the solution without violating energy inventory constraint in (12), and delay tolerance (subtour-elimination) constraints in (13) and (14) in the mE2-VRP. Therefore, the solution obtained by the c-DM algorithm is a feasible solution to the master mE2-VRP.

6. Numerical study

This section sets up numerical studies to validate the performance of the model and algorithm developed in the study. Built upon that, we further explore insights and the applicability of CaaS⁺ in citywide and statewide implementations. To do that, we conducted two sets of numerical experiments, which are respectively built upon the Chicago sketch network (Mayer, 1961), Fig. 7 (a), and the Florida statewide network, Fig. 7 (b). All numerical experiments are run on a DELL Precision 3630 Tower with 3.60 GHz of Intel Core i9-9900 k CPU, 8 cores and 16 GB RAM in a Windows environment.

The two sets of experiments share the default setting for some parameters of the EDs and the EPs. Specifically, the ED battery capacity is assumed to be 90 kWh, with consumption rate $\varpi = 0.4$ kWh/mile (max driving range of 225 miles), which corresponds to the battery performance of Tesla model S. We consider that CaaS⁺ will relax the range anxiety, so that people would feel comfortable to leave home or workplaces without having their cars fully charged. Therefore, the initial battery inventory of the EDs is randomly generated above the safety inventory (2 kWh), and below the energy required to complete the trip, so that each ED in this experiment needs to have at least one recharging service. The EP fleet has the same battery parameters as the EDs, except that each EP can carry more than one battery. The experiments have each EP equipped with two full batteries as the default setting, unless otherwise stated. We further assume a power transfer rate η of 50 kW, and a transfer efficiency of 0.9 in CaaS⁺ (Abdolmaleki et al., 2019; Afshar et al., 2021; Chakraborty et al., 2020; Ucer et al., 2019; Umesh et al., 2021).

6.1. Numerical study 1: Chicago sketch network

6.1.1. Experiment settings

We first conduct the experiments built on the Chicago sketch network. The objective of the experiments are as follows: (i) evaluate the computation performance of the c-DM algorithm, (ii) compare the performance of CaaS⁺ with the charging-station only strategy, (iii) examine the traffic impact of CaaS⁺ at the network level, and (iv) analyze CaaS⁺ performance under different input parameters. The Chicago sketch network as shown in Fig. 7 (a) consists of 933 nodes and 2,950 links. The network is developed by the Chicago Area Transportation Study (CATS) (Mayer, 1961). It is a realistic yet aggregated representation of the Chicago region. We use it as a testbed

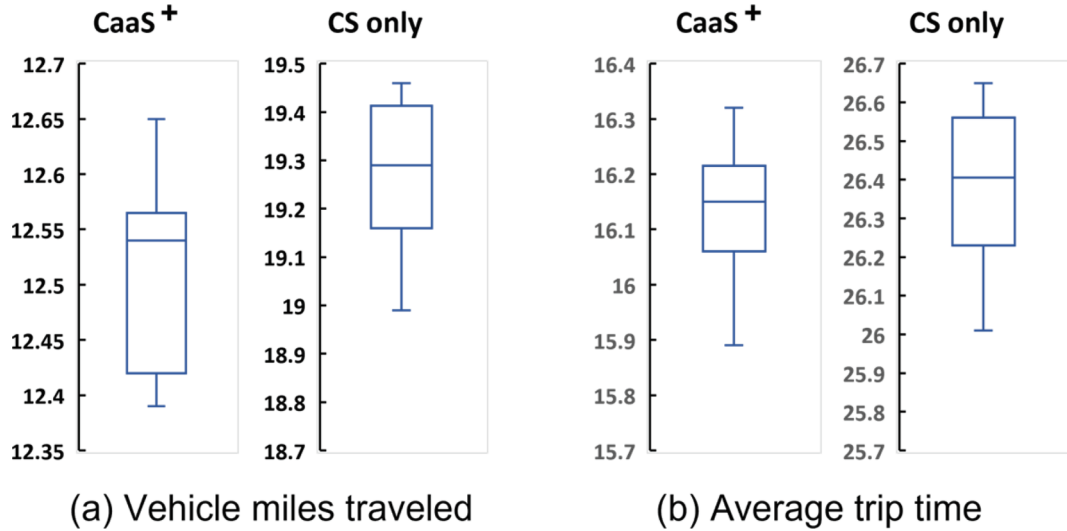


Fig. 8. Travel time and distance of co-using CaaS⁺/CS and the CS-only strategy.

to evaluate CaaS⁺ over citywide demands.

More exactly, the experiments simulate the ED trips from a field Chicago O-D trip dataset (Stabler et al., 2018), which consists of 1,260,910 trips. The average ED trip length is around 12 miles. We select the EP recharging depots (green nodes in Fig. 7 (a)) according to the Nissan dealers' locations in Chicago, because the dealers that sell electric vehicles usually have available chargers (Chen and Nie, 2015). Note that this study avoids the CBD area (red line) since it usually experiences heavy traffic and is not proper to set up CaaS⁺.

6.1.2. Computation performance of the c-DM algorithm

We first examine the computation performance of the c-DM algorithm under different instances with the size (the number of ED trips) varying from 60 to 10,000. We conducted 10 cases for each instance and summarized the results as average value of 10 runs in Table 2, in which the performance of the c-DM heuristic algorithm is compared with an existing commercial solver, Gurobi, in terms of the solution time and the EP fleet size (the objective function value; the smaller the better). Note that Gurobi is not efficient for the instance with larger sizes. Therefore, we set up solution time limits as an hour and two hours in Gurobi.

The results in Table 2 indicate that the Gurobi solver can only find a solution for an instance with a size less than 100 EDs within 2 h, but fails as the size of an instance is larger than 100 EDs. On the contrary, the c-DM algorithm finds comparable solutions for all the instances up to 10,000 with a more competitive computation efficiency. For example, the c-DM algorithm takes only a few seconds to find a solution for the instance with 100 EDs, and less than 15 min for the instance with 10,000 EDs. Moreover, the c-DM is able to find a solution with comparable optimality to that found by Gurobi within two hours for instances less than 100, and even better as compared with Gurobi's one-hour solution (e.g., 24 EPs by the c-DM vs 26 EPs by Gurobi solver for 100 EDs instance in Table 2). Therefore, the experiments confirmed that the c-DM algorithm addresses the scalability issue of the mE2-VRP model. This capability makes CaaS⁺ possible for an online application.

Beyond the fleet size, the experiments also record and analyze the EP service rate under different instances (the last column in Table 2), which is the ratio of the number of EDs to the EP fleet size. This service rate represents the number of EDs that one EP can serve on average. The results demonstrate that the EP service rate increases with the instance size and gets a plateau when the instance size is larger than 600 EDs. This is because the growth of instance size triggers more possibilities to develop a charging service coalition among ED itineraries. Thus, it renders a more flexible charging schedule for each EP to serve more EDs. Therefore, the EV usage and the service rate of CaaS⁺ present positive interaction and encourage each other's growth in a certain range of EV market penetration. Thus, CaaS⁺ does show the capability to cultivate the market from this perspective.

6.1.3. Travel time and distance saving for EDs

CaaS⁺ provides EDs an option to receive charging service on the move. It saves their detour trips to charging stations and the corresponding charging delay. We thus expect CaaS⁺ can save EDs' VTM and travel time. To demonstrate these benefits, our experiments compare those items in two scenarios.

- (i) The system co-uses CaaS⁺ and existing roadside Level-3 charging stations (CSs).
- (ii) Only using Level-3 CSs for charging services.

For scenario (i), we consider a proportion (p) of EV flow that originally uses charging station services will switch to the CaaS⁺ services (the EV penetration rate should be greater than p). To demonstrate the VTM and travel time saving of EDs by using the CaaS⁺, we randomly generate 10 instances. For each instance, we simulated 101,324 trips from the realistic Chicago O-D database. Among

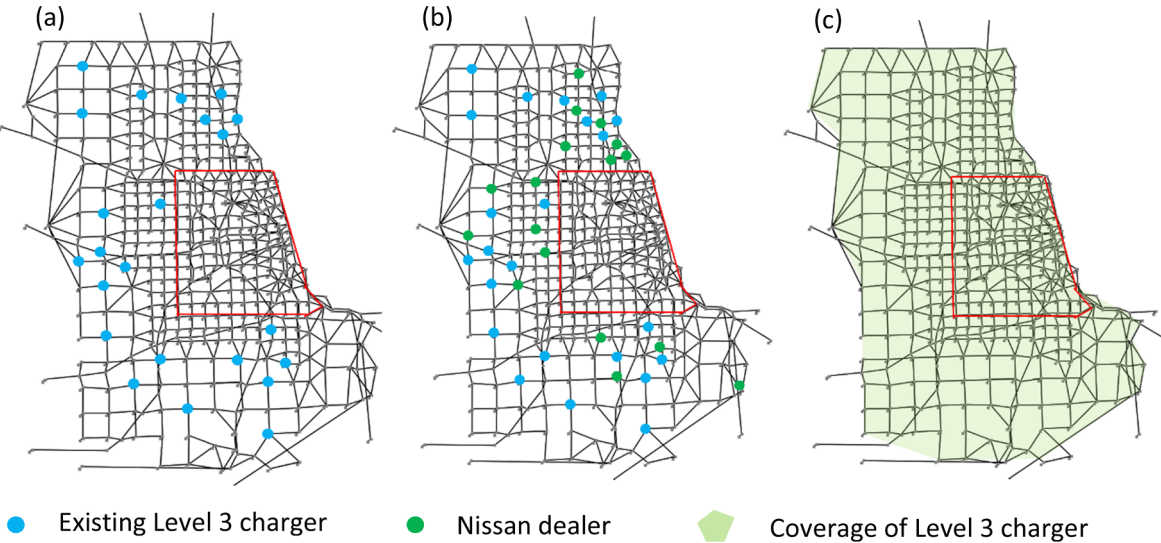


Fig. 9. Level 3 charging station coverage levels: (a) low coverage, 34% of existing gasoline charging stations; (b) medium coverage, 58% of that; (c) high coverage, no detour.

these trips, we select EDs as $p = 60\%$ of the trips to use the CaaS⁺ service, given that the CaaS⁺ service can be a supplement to charging station services to extend the coverage of charging stations. For the scenario of CS-only, we discarded those ED trips that do not have enough energy to reach the nearest charging stations during the trip. We further assume that there is no queue in the charging stations, and EDs only request the amount of energy that enables them to reach the destinations to make it consistent with the energy request for the CaaS⁺ service. The comparison metrics are EDs' averaged vehicle miles traveled (VMT) and averaged trip time in minutes. Fig. 8 (a) and (b) demonstrate EDs' average savings in VTM and trip time.

The results in Fig. 8 (a) show that using the CaaS⁺ service will help reduce ED's average VTM from 19 miles to 12.5 miles (i.e., save 50 % of the trip for an ED to finish the trip). Fig. 8 (b) demonstrates that ED's average trip time under the scenario of CS-only is around 26 min, while it is reduced to around 16 min under the scenario of co-using CS and CaaS⁺. Thus, we claim that CaaS⁺ saves about 40 % of ED's travel time from the CS-only service. It should be noted that this experiment sets up the most effective services at a charging station by taking away the queuing waiting time and minimizing charging time by limiting the battery request to the minimum level to complete a trip, etc. Therefore, the actual benefit of CaaS⁺ can be more significant in practice if we consider charging station queue and EV users may want to fully charge the batteries.

In short, the results in Fig. 8 indicate that CaaS⁺ provides a great solution in addition to existing charging station services. It may extend the service coverage to the distant demand and relieve charging station crowdedness. Note that even though these experiment results demonstrate the merit of CaaS⁺ to existing CS service, this does not indicate these two charging solutions are exclusive in reality. Our next section will show the weakness of CaaS⁺, such as the traffic overhead introduced by the EPs (the similar issue of the battery swapping). We would suggest co-using existing charging options so that we can serve diverse customers by using their strengths while avoiding their weaknesses.

6.1.4. System traffic overhead

The results in Table 2 shows that the necessary fleet size of the EPs increases with the number of EV users. It indicates the increase of traffic overhead. The last section indicates that CaaS⁺ saves EDs' detour trips for charging stations and reduces VTM per ED. Thus, it will mitigate congestion. In this section, we seek to study the mixed congestion effect of CaaS⁺ so that we can have a comprehensive understanding of its applicability in practice.

We set up our experiments in scenarios (i) and (ii) defined in section 6.1.3 under three different network congestion levels (i.e., the average ratio of traffic volume (v) to capacity (c) in the network). They include v/c respectively equal to 0.35 (low or no congestion), 0.60 (moderate congestion), and 0.80 (heavy congestion) (Xie et al., 2018). Those congestion levels are generated by randomly selecting the background traffic from the realistic Chicago O-D database until the desired v/c ratio is reached. Considering the coverage of charging stations are growing in the near future and it will affect EDs' detour trips, the experiments consider the low, medium, and extreme high charging station coverage levels, which respectively correspond to the cases that the number of Level-3 charging stations reaches to 34 %, 58 % of the existing gasoline charging station in Chicago, and extremely densely distributed so that EV can easily access charging stations without any detours. Fig. 9 provides an illustration. Specifically, Fig. 9(a) involves all Level-3 charging stations in Chicago according to PlugShare (PlugShare, 2022); Fig. 9(b) further involves the existing Nissan dealers in the city and Fig. 9(c) assumes that Level-3 charging stations are densely distributed and no detour is required for all EDs. For each scenario under a given congestion level and charging station coverage, we simulate 10 instances for each ED demand level. The parameters of all the experiments follow the default setting. Each EP is equipped with two 90 kWh batteries, e.g., the Tesla P90D battery. As 540 kg battery

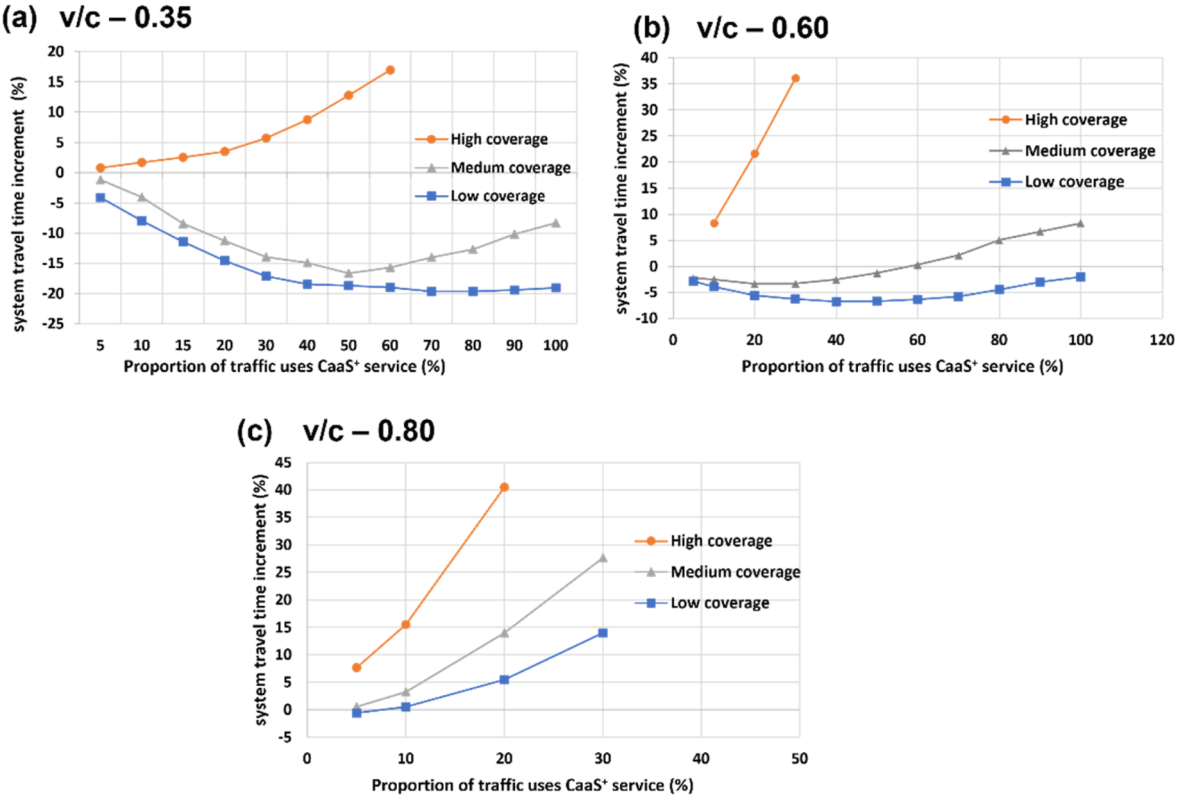


Fig. 10. Traffic overhead under three traffic scenarios: (a) - (c) traffic overhead vs demand size under different traffic congestion levels with different CS coverages.

weight gives a total weight of 1080 kg, EP is a small van with one passenger car unit (PCE) (Adnan, 2014).

The traffic congestion effect of EPs is evaluated by the percentage increase/decrease of the system travel time by involving CaaS⁺ in Equation (40).

$$\Delta \Sigma = \frac{\Sigma_E - \Sigma_0}{\Sigma_0} \times 100\%, \quad (40)$$

where Σ_0 is the system travel time by only using charging stations; Σ_E is the system travel time by co-using mE2 and charging station services. The link travel time is measured by the Bureau of Public Roads (BPR) function (Branston, 1976). Briefly, a proportion of the traffic in the network is selected as the EDs, which originally use charging station service but switch to the CaaS⁺ service as the new solution is available. Then, a fleet of EPs is dispatched according to the charging plans from the c-DM algorithm. The experiments will update the link volume, V_a by counting the reduction of EDs' detour trips and the increase of EP traffic. Built upon that, we compute the corresponding system travel time for all vehicles (except EPs).

The experimental results are summarized in Fig. 10. Specifically, Fig. 10(a) – (c) display the congestion effect of the EPs under different ED demand, CS coverage, and congestion levels. The results in Fig. 10(a) indicate that CaaS⁺ can serve the majority of EDs in the network while greatly improving the traffic efficiency by saving their detours (up to around 20 % decrease in system travel time), when the charging station coverage is under low or medium, and traffic is light (0.35 v/c). This is also consistent with the findings in Fig. 8. These benefits keep but decline from some points when the congestion and the station coverage increase. Fig. 10(b) shows that CaaS⁺ can serve the majority of EDs while mitigating congestion (up to 7 % travel time saving), when the CS coverage is low and the traffic is mildly congested (0.6 v/c). But this vantage starts to decline when it serves more than 60 % of the traffic flow with a medium level of charging station coverage. The results in Fig. 10(c) demonstrate that CaaS⁺ does not show the merit in reducing congestion when traffic is highly congested (0.8 v/c). Fig. 10 (a)-(c) all demonstrate that CaaS⁺ does not show an apparent advantage to charging stations in sustaining traffic efficiency, when the network is densely covered by charging stations. Under this case, our results show that CaaS⁺ can still act as an extension of the CS to save the charging delay of EDs and serve up to 50 % of the traffic flow under the 0.35 v/c traffic condition (or 18 % of the traffic flow under the 0.60 v/c traffic condition), given we select the tolerable traffic overhead as 15 %, which means a delay less than 3 min for a 20-minute trip.

6.1.5. EP energy inventory analysis

In practice, each EP can carry multiple batteries. Thus, individual EPs may have different initial energy inventories. They together

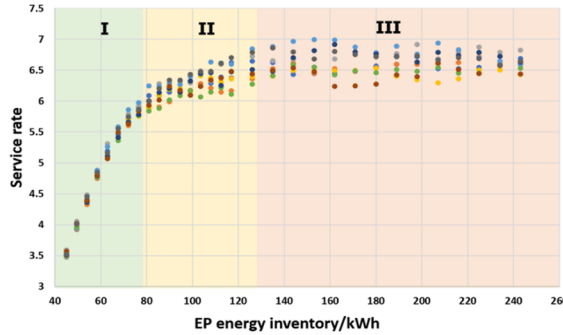


Fig. 11. Plot of EP service rate under the instances with different initial EP energy inventory. Different colors in Fig. 11 represent different instances.

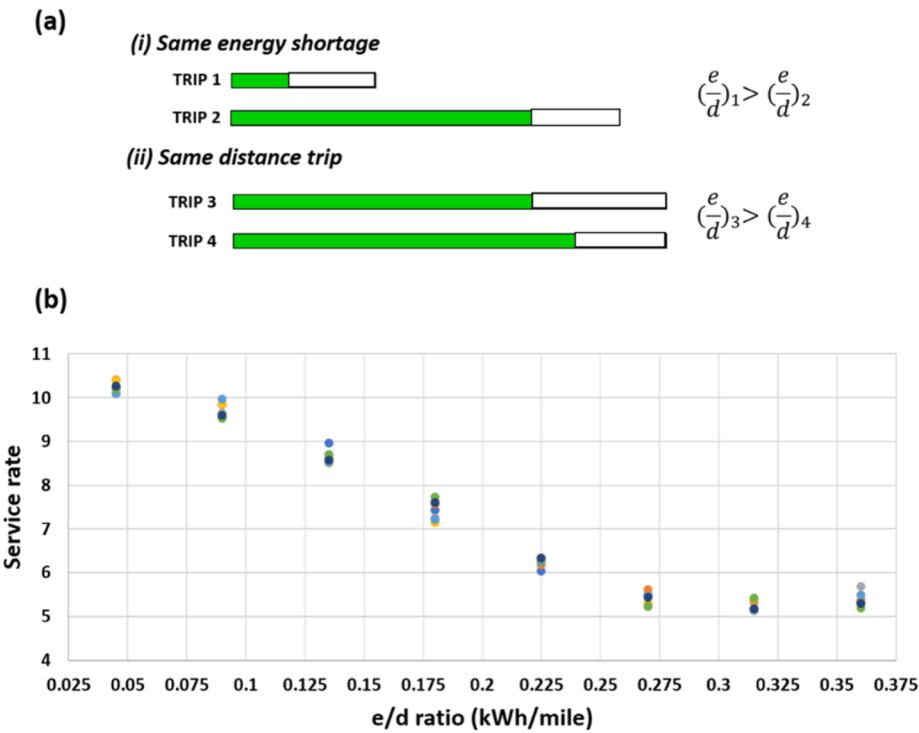


Fig. 12. (a) Schematic representation of the energy shortage of EDs; the length of each bar represents the length of the trip. The filled/unfilled section represents the remaining/shortage of battery; (b) EP service rates under different ED energy shortage rate. Different colors in Fig. 12 represent different instances.

will affect the service efficiency of CaaS⁺. It is valuable to test the sensitivity of CaaS⁺ performance to the initial energy inventory. The obtained insights can help develop strategic energy inventory control and improve service efficiency. To set up the experiment, we randomly generate and simulate 10 instances, each with an instance size of 10,000 EDs. We collect the EP service rate under the experiments with different initial energy inventories, varying from 36 kWh to 243 kWh, and then plot the results in Fig. 11 (a). Note that the capacity of one battery is 90 kWh.

The results in Fig. 11 (a) demonstrate that the service rate first grows with the increase of individual EP's initial energy inventory and then reaches a plateau when the inventory is above 130 kWh (about 1.4 battery). More precisely, the results present three phases (I-III). When the initial battery is less than 80 kWh, the service rate almost linearly grows with the increase of EP's initial energy inventory; after that, the effect slows down, and eventually reaches a plateau when we further increase the initial battery inventory above 130 kWh. This implies that the initial energy inventory only limits the service rate of an EP when it is relatively low. There are other factors to affect the service rate. We noticed that the EDs' itineraries and their inherent correlations play another important factor. For example, each ED service sets a given itinerary and service time window. Due to this limit, an EP may not be able to reach an ED timely even if it has enough energy inventory. Therefore, there exists an upper bound for the EPs' service rate as it presents in phase

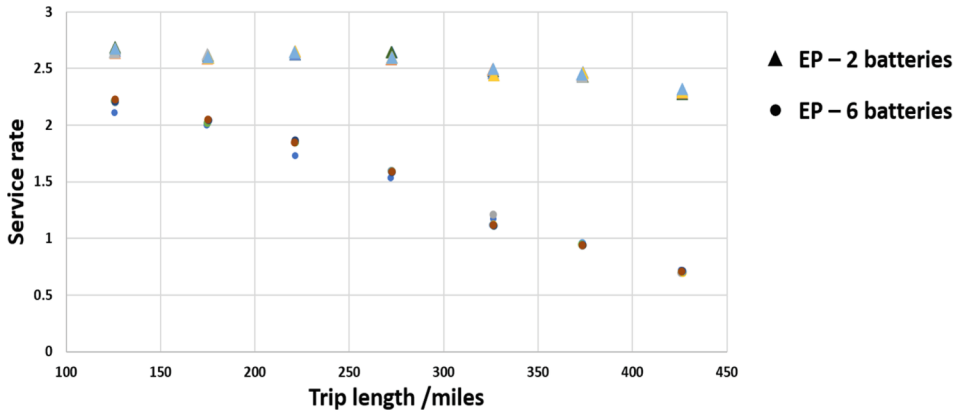


Fig. 13. Plot of EP service rate under the instances with different ED trip distance and each EP carrying different numbers of batteries. Different colors in Fig. 13 represent different instances.

III. In phase II, the service rate is limited by mixed factors and therefore, the plot exhibits a slower increase. The factor of the EDs' itineraries and their inherent correlations can also be evidenced by the much more spreading data points in the phases II and III.

More importantly, the results in Fig. 11 (a) imply that an EP is ready to go if its initial energy inventory is above 130 kWh. In other words, an EP does not have to be fully recharged for the next duty. Consequently, an EP can participate in the service in a new batch from the location in the previous service cycle without returning to a depot, if its remaining inventory is above 130 kWh. Accordingly, we can foresee that if each EP carries more than 2 batteries, it can reduce the times for returning to the depot and improve the service coverage by obtaining more opportunities to timely serve those EDs that are far away from depots, but close to the idle EPs from the last service cycle. This insight can help set up a more efficient CaaS⁺ and we have factored in these considerations in our model by allowing EPs to start from the current location (not limited to the depots) with the current energy inventory.

6.1.6. Range anxiety analysis

This study noticed that the energy shortages and trip lengths (range anxiety) of the EDs jointly affect the service efficiency of CaaS⁺. We demonstrate this observation by using the trips in Fig. 12(b) as examples. Given Trips 1 and 2 have the same energy shortage but different trip lengths. Our experiments showed that Trip 2 will potentially give more flexibility to schedule an EP trip than Trip 1 does since Trip 2 is longer and it can accommodate more chances to encounter an EP by either local or distant switch. On the other hand, Trips 3 and 4 have the same trip length, but Trip 4 needs less energy. Our experiments show that it is relatively easier to consolidate the service for Trip 4 with others served by an EP. Thus, Trip 4 will facilitate the service schedule better than Trip 3. With this view, we define the energy shortage rate (labeled as e/d ratio) by the ratio of the ED's energy shortage to its trip length, and then use the e/d ratio to quantify the collective effect. On the other hand, this e/d ratio provides a quantitative way to measure the range anxiety. Namely, a larger value of the e/d ratio indicates a higher level of range anxiety.

Accordingly, we conduct experiments to explore comprehensive insights for the effect of the e/d ratio on the service efficiency of CaaS⁺, in particular, the service rate. To do that, our experiments randomly generate 10 instances, each of which involves 10,000 EDs with an average e/d ratio such as 0.05 kWh/mile. The 10 instances cover the scenarios that the e/d ratio varies from 0.025 kWh/mile to 0.375 kWh/mile. All other parameters follow the default setting. From the results in Fig. 12 (c), we noticed that the EP service rate gets worse as the e/d ratio increases, but becomes stable when the e/d ratio is above 0.25 kWh/mile. This interesting observation gives a hint for CaaS⁺ to improve the service rate by developing some strategies, such as pricing and incentives, towards the ED's e/d ratio to guide EDs' energy requests to improve the service rate. For example, CaaS⁺ may charge more if an ED is with a higher e/d ratio, which will encourage the EDs to request the CaaS⁺ service when they have a small e/d ratio, and ultimately mitigate the range anxiety.

6.2. Numerical study 2: Florida statewide network

Numerical study 1 evaluates the performance of CaaS⁺ on a citywide network. The ED trips are all intra-city trips with 12 miles as the average trip length. However, existing studies show that statewide long-distance trips usually suffer from range anxiety more due to the battery range limitation and sparse charging service stations on the inter-city roads. With this view, CaaS⁺ can be a promising relief for long-distance travelers using EVs. This study therefore further tests the performance of CaaS⁺ at a state-level network.

We use Florida statewide network as the testbed. As shown in Fig. 7(b), the county-based network is with 63 nodes representing counties, big cities, important road junctions, or EP depots, and 260 links representing the connections. The potential EP recharging depots (green nodes) are selected based on the existing DC fast charging (DCFC) locations (FDOT, 2020). The statewide freight trips were obtained by running the simulation model, Florida Statewide Model v7.2 (FLSWM) (Zanjani et al., 2015). The average passenger trip distance is 231.3 miles, with a minimum of 22.5 miles and a maximum of 937.6 miles.

To analyze the impact of the trip distance on the performance of CaaS⁺, we categorize the passenger trips into seven classes in terms of their trip distances, [100, 150), [150, 200), [200, 250), [250, 300), [300, 350), [350, 400), [400, 450]. For each distance class, we

Table 3

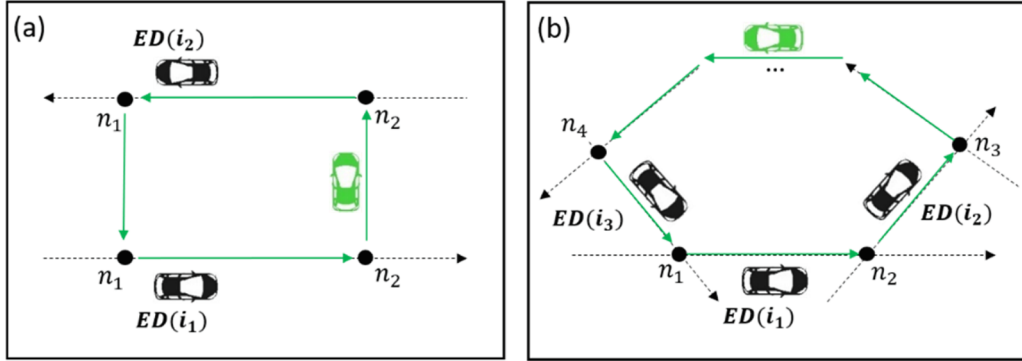
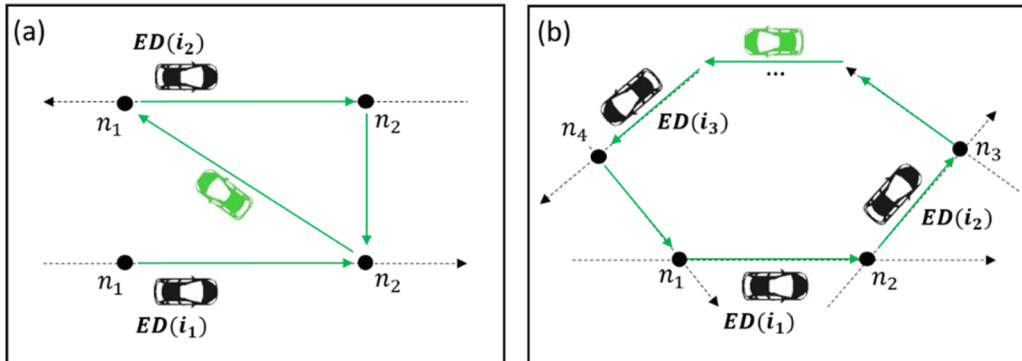
Parameters and Variables.

Notation	Explanation
1. Parameters in the mE2-VRP	
$H = \{h\}_{h=1}^H$	One service horizon, discretized into H time intervals.
$T > 0$	The length of the time interval.
$i \in \mathcal{D}_h$	Index and set (abbreviated as \mathcal{D}) of the EDs that depart during the h time interval.
$s \in \mathcal{S}_h$	Index and set (abbreviated as \mathcal{S}) of the EPs available at beginning of the h time interval.
D_n	A set of the EDs that pass through a node n .
\mathcal{N}	The set of nodes. $\mathcal{N} = N_0 \cup N_e \cup N_p \cup N$.
N_0	A set of the first available locations for service along the routes of the EDs.
N_e	A set of the destinations of the EDs.
N_p	A set of depots of the EPs.
$n \in N$	Index and set of encounter nodes between the EDs.
N_i	A set of encounter nodes along the route of ED(i).
\mathcal{N}_i	A set of nodes to represent the route of ED(i), $\mathcal{N}_i = (i_0, N_i, i_e)$.
$A_i \subseteq A$	A set of arcs to represent the route of ED(i).
a_n^i	The arc starting from node n on the route of ED(i). a_n^i is replaced by $a^i(n)$ in some formulations.
$i_0 \in N_0$	Index and set of origin of the EDs.
$i_e \in N_e$	Index and set of destination of the EDs.
s_0	Index of depots/current locations of the idle EPs.
p_n	Index of the nearest depot from node n . $p_n \in N_p$.
\tilde{t}_0^i	The estimated arrival time of ED(i) at i_0 .
$\bar{\tau}_i$	The maximum endurable waiting time of ED(i) at i_0 .
\bar{e}_i	The battery capacity of ED(i).
e_0^i	The estimated battery level of ED(i) at i_0 .
ϖ_i	The energy consumption rate of ED(i).
e_{-d}	The safety energy inventory of the EDs.
e_{ia}^-	The energy that ED(i) losses on the arc a .
\bar{e}_{ia}^+	The maximum energy that ED(i) can receive from the EPs on arc a .
e_0^s	The initial energy inventory of EP(s).
ϖ_s	The energy consumption rate of ED(s).
e_{-s}	The safety energy inventory of the EPs.
$e_{n \rightarrow m}^-$	The energy consumed for the EPs to travel from node n to m .
η	The mE2 power transfer rate of the EPs.
e_{sa}^-	The energy that EP(s) losses on the arc a .
$t_{n \rightarrow m}$	The average travel time from node n to node m .
2. Variables in the mE2-VRP	
F	Optimization objective of the mE2-VRP.
$z_{i,a}^s$	Binary variable to identify whether EP(s) serves ED(i) on the arc a . If true, $z_{i,a}^s = 1$, otherwise $z_{i,a}^s = 0$, $\forall s \in \mathcal{S}, i \in \mathcal{D}, a \in A_i$. $Z = \{z_{i,a}^s\}$ is the set.
$o_i^{n,s}$	Binary variable to identify whether EP(s) travels from depot to charge the ED(i) at node n . If true, $o_i^{n,s} = 1$, otherwise $o_i^{n,s} = 0$, $\forall s \in \mathcal{S}, i \in \mathcal{D}, n \in \mathcal{N}_i \setminus i_0$. $O = \{o_i^{n,s}\}$ is the set.
$q_i^{n,s}$	Binary variable to identify whether EP(s) leaves ED(i) and return to depot from node n . If true, $q_i^{n,s} = 1$, otherwise $q_i^{n,s} = 0$, $\forall s \in \mathcal{S}, i \in \mathcal{D}, n \in \mathcal{N}_i \setminus i_0$. $Q = \{q_i^{n,s}\}$ is the set.
$u_{i,j}^{n,s}$	Binary variable to identify whether EP(s) conducts local switches from ED(i) to ED(j) at node n . If true, $u_{i,j}^{n,s} = 1$, otherwise $u_{i,j}^{n,s} = 0$, $\forall s \in \mathcal{S}, i \in \mathcal{D}, n \in \mathcal{N}_i \setminus i_0, j \in D_n, j \neq i$. $U = \{u_{i,j}^{n,s}\}$ is the set.
$v_{i,j}^{n,m,s}$	Binary variable to identify whether EP(s) conducts distant switch from ED(i) at node n to ED(j) at node m . If true, $v_{i,j}^{n,m,s} = 1$, otherwise $v_{i,j}^{n,m,s} = 0$, $\forall s \in \mathcal{S}, i, j \in \mathcal{D}, i \neq j, n \in \mathcal{N}_i \setminus i_0, m \in \mathcal{N}_j \setminus i_0, n \neq m$. $V = \{v_{i,j}^{n,m,s}\}$ is the set.
$w_i^{n,s}$	Binary variable to identify whether EP(s) charges ED(i) on the arc $a(i, n) - 1$ and continue to charge ED(i) on the arc $a^i(n)$. If true, $w_i^{n,s} = 1$, otherwise $w_i^{n,s} = 0$, $\forall s \in \mathcal{S}, i \in \mathcal{D}, n \in N_i$. $W = \{w_i^{n,s}\}$ is the set.
e_{ia}^+	Continuous variable represents the energy that ED(i) receives from the EPs on arc a , $\forall i \in \mathcal{D}, a \in A_i$.
e_i^i	Continuous variable represents the energy inventory of ED(i) at node n , $\forall i \in \mathcal{D}, n \in \mathcal{N}_i \setminus i_0$.
τ_i	Continuous variable represents the waiting time of ED(i) at i_0 , $\forall i \in \mathcal{D}$.
t_0^i	Continuous variable represents the actual departure time of ED(i), $\forall i \in \mathcal{D}$. $t_0^i = \tilde{t}_0^i + \tau_i$.
t_n^i	Continuous variable represents the arrival time of ED(i) at node n , $\forall i \in \mathcal{D}, n \in \mathcal{N}_i$. $t_n^i = \tilde{t}_0^i + t_{i,n} + \tau_i$.
E_s	Continuous variable represents the total energy consumed for EP(s), $\forall s \in \mathcal{S}$.
$\gamma_{i,a}$	Continuous auxiliary variable to linearize the non-linear term of $e_{ia}^+ (\sum_{s \in \mathcal{S}} z_{i,a}^s)$, $\forall i \in \mathcal{D}, a \in A_i$.
$\zeta_{i,a}$	Continuous auxiliary variable to linearize the non-linear term of $z_{i,a}^s e_{ia}^+$, $\forall i \in \mathcal{D}, a \in A_i$.
3. Parameters and variables in the c-DM algorithm	
$J_{i,n}$	Local-Switch Candidate set of ED(i) at node n $\forall i \in \mathcal{D}, n \in \mathcal{N}_i \setminus i_0$.
$p(i,j)$	Number of times that an EP can do local switch from ED(i) to ED(j) along the route of ED(i).
P	Coalition potential matrix, $P = [p(i,j)]_{i,j \in D}$.
\mathcal{S}_0	A set of EPs that are dispatched in the initial solution.
\mathcal{S}_s^*	The set of the EDs serviced by EP(s) in the initial feasible solution.
$s(n)$	The n -th ED served by EP(s) in the initial feasible solution. $s(-1)$ is the last ED served by EP(s).

(continued on next page)

Table 3 (continued)

Notation	Explanation
E_s^*	The total energy losses (exclude idle energy losses from depot to the first customer and from the last customer to the depot) of EP(s) in the initial feasible solution.
t_0^{*s}	The time that EP(s) starts charging the first customer in the initial feasible solution.
t_e^{*s}	The time that EP(s) leaves the last customer in the initial feasible solution.
$H(s)$	The seed tour indexed by the EP(s) in the initial feasible solution, $\forall s \in \mathcal{S}_0$, which is a tuple, $H(s) = (n, t_0^{*s}, m, t_e^{*s}, E_s^*)$, and records the locations and time that EP(s) starts servicing the first customer and completing service with the last customer as well as the total energy losses.

**Fig. 14.** illegal subtour with size (a) $n = 2$ and (b) $n \geq 3$, that is formed by local switches only.**Fig. 15.** illegal subtour formed by distant and local switches with size (a) $n = 2$ and (b) $n \geq 3$.

generate 10 instances by selecting 10,000 qualified trips from the passenger trip dataset. All parameters follow the default setting, except that the EPs can carry either 2 batteries (180 kWh capacity) or 6 batteries (540 kWh capacity).

Fig. 13 displays the plots of EP service rate vs the ED trip distance under different two scenarios, in which an EP is equipped with 2 or 6 batteries, respectively. The results indicate that the max EP service rate is around 2.5 and it declines further as the length of individual ED's trip increases. Equipped with more batteries helps to improve service efficiency. However, a six-battery pack gives a total weight of 3,240 kg, so the EP has to be a light-duty truck with 3 PCE (Adnan, 2014). Thus, we conclude that using CaaS⁺ to serve state-wide trips may cause more traffic than it does for citywide trips. This is consistent with our common sense. The long-distance EDs (such as trucks) usually require more energy, while each EP can only carry limited batteries. Moreover, the EPs usually travel longer distances to provide statewide service and then return the depots. Therefore, they experience more idle energy losses. In conclusion, these results imply that building more charging stations (depots) and providing CaaS⁺ around the depots will benefit service efficiency on the statewide service. Moreover, the results also suggest using a pricing strategy according to the EDs' trip lengths and energy requests will balance the service quality, operation cost, and system traffic impacts.

7. Conclusion

This paper introduces CaaS⁺ that provides the charging services for EVs on the move so that we can relieve the range anxiety and charging delay of EDs by taking advantage of the mE2 technology. Mathematically, CaaS⁺ is modeled as a mE2-VRP model, which is a mixed-integer program that seeks to explore the optimal routing schemes so that we can dispatch the commercial electricity suppliers

(i.e., EPs) to charge EVs with the low level of batteries (i.e., EDs) when both of them are on the move while minimizing the extra traffic introduced by EPs. The model development addressed the challenges raised by the unique features of the on-the-move electricity delivery. Moreover, we contribute a new heuristic algorithm (i.e., the c-DM algorithm) to efficiently solve a large-scale mE2-VRP by integrating clustering and parallel computation with commercial optimization solver. The efficiency and applicability of our approaches are accessed by the numerical experiments built upon the Chicago city network and Florida state network.

Our experiments show that the proposed heuristic addresses the scalability of the mE2-VRP model and makes it possible to approach CaaS⁺ with realistic settings under different traffic circumstances. Our experiments further show that because of the elimination of detours for EDs, CaaS⁺ significantly saves the EDs' trip distance and time compared with scenarios where the charging station is the only available service. Even though CaaS⁺ introduces extra traffic by dispatching the EPs, but the results indicate this traffic overhead is compensated by the EDs' detour savings and CaaS⁺ saves travel time up to 20 % (or 7 %) in a light (or moderate) traffic environment. Thus, as a supplement to the existing charging options, CaaS⁺ is a promising and applicable solution to cultivate the mainstream adoption of EVs in the future. Last, we conducted sensitivity analyses on the operational inputs of CaaS⁺. The results demonstrate that CaaS⁺ may maintain a high service efficiency by setting the initial energy inventory of the EPs above 130 kWh since it avoids frequent recharging trips. More importantly, CaaS⁺ may lead to less traffic overhead if the majority of the EDs are served when they are under a lower energy shortage. CaaS⁺ performs better for the EDs with shorter intercity trips than those conducting longer statewide trips. These observations together suggest using certain strategies, such as incentives and pricing, according to EDs' energy requests and trip lengths can guide service requests of EDs to improve the service efficiency.

This study is among the early efforts to study the on-the-move charging service to relieve range anxiety and promote the usage of EVs. Several potential future research can be further explored from this study. For example, we will investigate the operation of CaaS⁺ while integrating the depot location planning and pricing strategies. We noticed that travel time and energy usage often present stochastic features. Future research will consider these factors and make the mE2-VRP can accommodate the uncertainty in reality. Those extensions will make CaaS⁺ work more efficiently, but also complicate the existing models and raise new computation challenges. Our future work will address them. Furthermore, it is a promising research direction to couple CaaS⁺ with other on-demand services, such as taxi and package delivery, which is a more complicated vehicle routing problem.

Authors contributions

The authors confirm the contributions to the paper as follows. Dr. Du initiated the research idea and led the main methodologies development. Under the supervision of Dr. Du, Ph.D. student Jiahua Qiu contributed to the development of the technical details in the mE2-VRP, c-DM algorithm design, and numerical experiments. All authors edited and reviewed the results and approved the manuscript's final version.

Declaration of Competing Interest

The authors declare that they have no known competing financial interests or personal relationships that could have appeared to influence the work reported in this paper.

Acknowledgment

This study is partially supported by National Science Foundation, award CMMI 1818526 (Previous: 1554559).

Appendix A. Nomenclature

Appendix B. Algorithm 1: Building encounter network

```

Input:  $r_i = [n_{i1}, l_{i12}, n_{i2}, \dots, l_{i(m-1)i_m}, n_{im}], \forall i \in \mathcal{D}$ 
Initialize: Encounter node set  $N \leftarrow \{\}$ 
1. For all  $i, j \in \mathcal{D}$  do
2.    $p_i \leftarrow 1; p_j \leftarrow 1$ 
3.   While  $p_i < size(r(i))$  and  $p_j < size(r(j))$  do
4.     if  $l_i = l_j$ , then  $N \leftarrow N \cup \{\tilde{n}_i\}; p_i \leftarrow p_i + 2; p_j \leftarrow p_j + 2$ 
5.     else:  $p_i \leftarrow p_i + 2$ 
6.    $p_i \leftarrow 0; p_j \leftarrow 0$ 
7.   While  $p_i < size(r(i))$  and  $p_j < size(r(j))$  do
8.      $n_i \leftarrow r_i[p_i]; n_j \leftarrow r_j[p_j]$ 
9.     if  $n_i = n_j$  and  $L_{-i} = L_{-j}$  and  $l_{i+} = l_{j+}$ 
10.      then  $N \leftarrow N \cup \{n_i\}; p_i \leftarrow p_i + 2; p_j \leftarrow p_j + 2$ 
11.      else:  $p_i \leftarrow p_i + 2$ 
12  return  $N$ 
```

The algorithm takes the physical routes of each ED(i) as input r_i . Each route is represented by a list of nodes and links visited by the ED in order. For each pair of ED(i) and ED(j), the algorithm considers the two scenarios: (i) the two EDs' routes have link overlaps, and (ii) the two EDs' routes cross at nodes (i.e., traffic intersection). For scenario (i), a virtual node representing each overlap link will be considered as an encounter node and added to the encounter node set N. For scenario (ii), each crossed node will be considered as an encounter node and added to the set N. The algorithm will scan through the route list of each ED pair only once, so the time complexity of the algorithm is $O(n^2r)$ where n is the number of EDs and r is the maximum possible length of ED's route.

Appendix C. Algorithm 2: Clustering algorithm

```

Initialize: cluster index  $c \leftarrow 0$ 
Input:  $p(i,j), \forall i,j \in \mathcal{S}$ 
1   While  $(p(i,j) \neq 0, \forall i,j)$  do
2      $c \leftarrow c + 1$ 
3      $i \leftarrow \text{argmax}_i[p(i,j)], \text{Construct cluster } \mathcal{C}(c) = \{i\}; p(j,i) = 0, \forall j$ 
4      $j \leftarrow \text{argmax}_j[p(i,j)]$ 
5     While  $(p(i,j) > 1)$  do
6        $\mathcal{C}(c) \leftarrow \mathcal{C}(c) \cup \{j\}$ 
7        $p(k,j) = 0, \forall k$ 
8        $i \leftarrow j; j \leftarrow \text{argmax}_k[p(i,k)]$ 
9   return  $\mathcal{C}$ 

```

The algorithm starts with the largest entry $p(i,j)$ in the coalition potential matrix P to construct the first cluster $\mathcal{C}(1) = \{i,j\}$. ED(i) and ED(j) are in one cluster because ED(j) has a great potential to be served next by an EP doing local switch from ED(i). Now as both ED(i) and ED(j) are clustered, they cannot present in other clusters. Accordingly, the algorithm zeros the i -th and j -th column of the CP-matrix. Next, the algorithm moves to the row j , and searches for the largest entry to include the next ED to the cluster $\mathcal{C}(1)$. As the largest entry is searched, this ED has the highest potential to be serviced after ED(j). As the algorithm repeats the searching process, the cluster $\mathcal{C}(1)$ is settled until no more ED can be clustered into $\mathcal{C}(1)$. Then, the algorithm searches the largest entry in the updated CP-matrix and repeats the whole procedure to construct other clusters. Finally, the clustering algorithm returns a set of clusters, $\mathcal{C}(c)$, $\forall c$. For convenience, we denote the set of EDs that are associated with the cluster $\mathcal{C}(c)$ as \mathcal{S}_c .

Appendix D. Algorithm 3: Merging algorithm

```

Input:  $H(s), \forall s \in \mathcal{S}_0$ 
1   Create initial seed tours,  $H(\mathcal{S}_0) = (H(s), \forall s \in \mathcal{S}_0)$  by solving sub-mE2-VRP( $c$ ),  $\forall c$ .
2   for  $s \in \mathcal{S}_0$  do
3     for  $l \in \mathcal{S}_0$  do
4       if  $H(s) \vee H(l)$  then
5          $l^* \leftarrow l; t_e^{s-l} \leftarrow \max\{t_e^{*s} + t_{n_2 \rightarrow m_1(l)}, t_0^{*l}\} + t_e^{*l} - t_0^{*l}$ 
6         for  $k \in \mathcal{S}_0$  do
7           if  $H(s) \vee H(k)$  and  $t^* > \max\{t_e^{*s} + t_{n_2 \rightarrow m_1(k)}, t_0^{*k}\} + t_e^{*k} - t_0^{*k}$  then
8              $l^* \leftarrow k; t_e^{s-l^*} \leftarrow \max\{t_e^{*s} + t_{n_2 \rightarrow m_1(k)}, t_0^{*k}\} + t_e^{*k} - t_0^{*k}$ 
9         Merge  $H(s)$  with  $H(l^*)$ ;  $H(s) \leftarrow \bar{H}(s-l^*)$ 
10         $\mathcal{S}_0 \leftarrow \mathcal{S}_0 \setminus \{l^*\}$ 
11   return  $H(\mathcal{S}_0)$ 

```

* $H(s) \vee H(l)$ indicates that tour $H(s)$ can merge with tour $H(l)$ by EP(s).

Mainly, a set of seed tours $H(\mathcal{S}_0) = (H(s), \forall s \in \mathcal{S}_0)$ is solved from sub-mE2-VRP(c) (Line 2). Next, for any tour $H(s) \in H(\mathcal{S}_0)$, we consider tour $H(l^*)$ has the highest priority to be merged with $H(s)$ by EP(s), if $H(l^*)$ leads to the smallest departure time in the merged tour $\bar{H}(s-l^*)$ (Line 4–9). For example, the time that EP separates from the last customer is $t_e^{s-l} = \max\{t_e^{*s} + t_{n_2 \rightarrow m_1(l)}, t_0^{*l}\} + t_e^{*l} - t_0^{*l}$ in the merged tour $\bar{H}(s-l) = H(s) \vee H(l)$. The algorithm compares t_e^{s-l} when $H(s)$ merges with different $H(l) \in H(\mathcal{S}_0)$ and selects $H(l^*)$ with the smallest $t_e^{s-l^*}$ to be merged with $H(s)$. After merging two seed tours, we update the tour information as $\bar{H}(s-l^*) = (n_1, t_0^{*s}, m_2, t_e^{s-l^*}, \bar{E}_s^*)$, where $\bar{E}_s^* = E_s^* + e_{n_2 \rightarrow m_1} + E_l^*$, which is the total energy consumed for EP(s) to serve all demands in both seed tours. And the departure time, $t_e^{s-l^*}$ is updated by Equation (41).

$$t_e^{s-l^*} = \max\{t_e^{*s} + t_{n_2 \rightarrow m_1}, t_0^{*l}\} + t_e^{*l} - t_0^{*l} \quad (41)$$

Also,

$$\Delta\tau_i = \begin{cases} 0, & \text{if } t_e^{*s} + t_{n_2 \rightarrow m_1} \leq t_0^{*l} \\ t_e^{*s} + t_{n_2 \rightarrow m_1} - t_0^{*l}, & \text{if } t_e^{*s} + t_{n_2 \rightarrow m_1} > t_0^{*l} \end{cases} \quad (42)$$

Finally, the tour $H(l^*)$ is removed from tours set $H(\mathcal{S}_0)$ and the process is repeated until no more tours can be merged.

Appendix E. Proof of Lemma 2 and 3

Lemma 2. For any $ED(i)$, a trip satisfying (13) and (14) eliminates subtours that are only formed by local switch from/back to $ED(i)$.

Proof. We also prove Lemma 2 by showing contradiction. Similar to the proof of Lemma 1, we first show that constraints (13) and (14) eliminate an illegal subtour formed by multiple local switches, when it only involves 2 EDs ($n = 2$). Then, the proof is extended to the case involving more than 2 EDs ($n \geq 3$). Suppose there exists an illegal subtour purely formed by local switches with $n = 2$. Fig. 14(a) shows an example. An EP first serves $ED(i_1)$ as they move together from node n_1 to node n_2 , and then it locally switches to serve $ED(i_2)$ starting from node n_2 (local switch: $u_{i_1,i_2}^{n_2,s} = 1$) until arriving at node n_1 . After that, the EP revisits $ED(i_1)$ at node n_1 (local switch: $u_{i_2,i_1}^{n_1,s} = 1$). We have (43) and (44) below, given that constraint (13) is satisfied with $u_{i_1,i_2}^{n_2,s} = u_{i_2,i_1}^{n_1,s} = 1$,

$$t_{i_2}^{n_2} - t_{i_1}^{n_2} \geq 0 \quad (43)$$

$$t_{i_1}^{n_1} - t_{i_2}^{n_1} \geq 0 \quad (44)$$

Adding (43) and (44), we have (47) below.

$$0 > (t_{i_2}^{n_2} - t_{i_1}^{n_1}) + (t_{i_1}^{n_1} - t_{i_2}^{n_2}) \geq 0 \quad (45)$$

which leads to the contradiction. Therefore, such subtour does not exist in a feasible solution of mE2-VRP because constraint (13) will be violated.

When $n \geq 3$ (see Fig. 14(b)), we assume an EP serves $ED(i_1)$ from node n_1 to node n_2 , and then it locally switches to serve $ED(i_2)$ starting from node n_2 (local switch: $u_{i_1,i_2}^{n_2,s} = 1$) to node n_3 . Next, it locally switches to serve other EDs until it serves $ED(i_3)$ from node n_4 to node n_1 . And finally, the EP revisits $ED(i_1)$ at node n_1 (local switch: $u_{i_3,i_1}^{n_1,s} = 1$). To show such subtour does not exist in a feasible solution, we only need to prove at least one of the local switches involved in the subtour is infeasible (violates constraint (13)). Without loss of generality, we only focus on two local switches from $ED(i_1)$ to $ED(i_2)$ at node n_2 , and $ED(i_3)$ to $ED(i_1)$ at node n_1 and assume all other local switches are feasible. We have (46)(47) below, given that constraint (13) is satisfied with $u_{i_1,i_2}^{n_2,s} = u_{i_3,i_1}^{n_1,s} = 1$,

$$t_{i_2}^{n_2} - t_{i_1}^{n_2} \geq 0 \quad (46)$$

$$t_{i_1}^{n_1} - t_{i_3}^{n_1} \geq 0 \quad (47)$$

Adding (46) and (47), we have (48) below,

$$0 \geq (t_{i_1}^{n_2} - t_{i_1}^{n_1}) + (t_{i_3}^{n_1} - t_{i_2}^{n_2}) > 0 \quad (48)$$

which leads to a contradiction. The subtour does not exist, which completes the proof.

Lemma 3. For any $ED(i)$, a trip satisfying (13) and (14) eliminates subtours that are formed by distant switch from/back to and local switch back to/from $ED(i)$.

Proof. We also prove Lemma 3 by showing contradiction. Similar with the proof of Lemma 1 and 2, we first show that constraints (13) and (14) eliminate an illegal subtour formed by multiple local and distant switches, when it only involves 2 EDs ($n = 2$). Then, the proof is extended to the case involving more than 2 EDs ($n \geq 3$). Suppose there exists an illegal subtour formed by distant and local switches with $n = 2$, see Fig. 15(a). Both $ED(i_1)$ and $ED(i_2)$ travel from node n_1 to node n_2 . An EP first serves $ED(i_1)$ from node n_1 to node n_2 , and then it travels back to node n_1 and conducts distant switch ($v_{i_1,i_2}^{n_2,n_1,s} = 1$) to serve $ED(i_2)$ from node n_1 until arriving at node n_2 . After that, the EP revisits $ED(i_1)$ at node n_2 (local switch: $u_{i_2,i_1}^{n_2,s} = 1$). We have (49)(50) below, given that constraint (13) and (14) are satisfied with $u_{i_2,i_1}^{n_2,s} = v_{i_1,i_2}^{n_2,n_1,s} = 1$,

$$t_{i_2}^{n_1} - t_{i_1}^{n_2} - t_{n_2 \rightarrow n_1} \geq 0 \quad (49)$$

$$t_{i_1}^{n_2} - t_{i_2}^{n_2} \geq 0 \quad (50)$$

Adding (49)(50), we have (51) below,

$$-t_{n_2 \rightarrow n_1} \geq (t_{i_1}^{n_2} - t_{i_2}^{n_1}) + (t_{i_2}^{n_2} - t_{i_1}^{n_1}) > 0 \quad (51)$$

(51) indicates that $t_{n_2 \rightarrow n_1} < 0$ which contradicts with $t_{n_2 \rightarrow n_1} > 0$. Therefore, such subtour does not exist in a feasible solution of mE2-VRP because constraints (13) and (14) will be violated.

When $n \geq 3$ (see Fig. 15(b)), we assume an EP serves $ED(i_1)$ from node n_1 to node n_2 , and then it locally switches to serve $ED(i_2)$ starting from node n_2 (local switch: $u_{i_1,i_2}^{n_2,s} = 1$) to node n_3 . Next, it conducts local or distant switches to serve other EDs until it serves $ED(i_3)$ and arrives at n_4 . And finally, the EP revisits $ED(i_1)$ at node n_1 by distant switch from node n_4 to node n_1 (distant switch: $v_{i_3,i_1}^{n_4,n_1,s} = 1$). To show such subtour does not exist in a feasible solution, we only need to prove at least one of the local or distant switches involved in the subtour is infeasible (violates constraints (13) and (14)). Without loss of generality, we only focus on the local switch from $ED(i_1)$ to $ED(i_2)$ at node n_2 , and distant switch from $ED(i_3)$ at node n_4 to $ED(i_1)$ at node n_1 and assume all other switches are

feasible. We have (52)(53) below, given that constraint (13) and (14) are satisfied with $u_{i_1, i_2}^{n_2, s} = v_{i_3, i_1}^{n_4, n_1, s} = 1$,

$$t_{i_2}^{n_2} - t_{i_1}^{n_2} \geq 0 \quad (52)$$

$$t_{i_1}^{n_1} - t_{i_3}^{n_4} - t_{n_4 \rightarrow n_1} \geq 0 \quad (53)$$

Adding (52)(53), we have (54) below,

$$-t_{n_4 \rightarrow n_1} \geq (t_{i_1}^{n_2} - t_{i_1}^{n_1}) + (t_{i_3}^{n_4} - t_{i_2}^{n_2}) > 0 \quad (54)$$

(54) indicates that $t_{n_4 \rightarrow n_1} < 0$ which contradicts with $t_{n_4 \rightarrow n_1} > 0$. Therefore, such subtour does not exist, which completes the proof.

References

- Abdolmaleki, M., Masoud, N., Yin, Y., 2019. Vehicle-to-vehicle wireless power transfer: Paving the way toward an electrified transportation system. *Transp. Res. Part C Emerg. Technol.* 103, 261–280.
- Adnan, M., 2014. Passenger car equivalent factors in heterogenous traffic environment—are we using the right numbers? *Proc. Eng.* 77, 106–113.
- Afshar, S., Macedo, P., Mohamed, F., Disfani, V., 2021. Mobile charging stations for electric vehicles—A review. *Renew. Sustain. Energy Rev.* 152, 111654.
- Baldacci, R., Bartolini, E., Mingozzi, A., 2011. An exact algorithm for the pickup and delivery problem with time windows. *Oper. Res.* 59, 414–426.
- Bongiovanni, C., Kaspi, M., Geroliminis, N., 2019. The electric autonomous dial-a-ride problem. *Transp. Res. B Methodol.* 122, 436–456.
- Braekers, K., Caris, A., Janssens, G.K., 2014. Exact and meta-heuristic approach for a general heterogeneous dial-a-ride problem with multiple depots. *Transp. Res. B Methodol.* 67, 166–186.
- Branston, D., 1976. Link capacity functions: A review. *Transp. Res.* 10, 223–236.
- Bulut, E., Kisacikoglu, M.C., 2017. Mitigating range anxiety via vehicle-to-vehicle social charging system. In: In: 2017 IEEE 85th Vehicular Technology Conference. (VTC Spring). pp. 1–5.
- Chakraborty, P., Parker, R., Hoque, T., Cruz, J., Bhunia, S., 2020. P2C2: Peer-to-Peer Car Charging, in: 2020 IEEE 91st Vehicular Technology Conference (VTC2020-Spring). pp. 1–5.
- Chakraborty, P., Parker, R., Hoque, T., Cruz, J., Du, L., Wang, S., Bhunia, S., 2022. Addressing the range anxiety of battery electric vehicles with charging en route. *Sci. Rep.*
- Chen, Z., Li, X., Zhou, X., 2019. Operational design for shuttle systems with modular vehicles under oversaturated traffic: Discrete modeling method. *Transp. Res. B Methodol.* 122, 1–19.
- Chen, P.W., Nie, Y.M., 2015. Stochastic optimal path problem with relays. *Transp. Res. Procedia* 7, 129–148.
- Cordeau, J.-F., Laporte, G., 2003. A tabu search heuristic for the static multi-vehicle dial-a-ride problem. *Transp. Res. B Methodol.* 37, 579–594.
- Cordeau, J.-F., Laporte, G., 2007. The dial-a-ride problem: models and algorithms. *Ann. Oper. Res.* 153, 29–46.
- Cui, S., Zhao, H., Chen, H., Zhang, C., 2018a. The mobile charging vehicle routing problem with time windows and recharging services. *Comput. Intell. Neurosci.* 2018.
- Cui, S., Zhao, H., Zhang, C., 2018b. Multiple types of plug-in charging facilities' location-routing problem with time windows for mobile charging vehicles. *Sustainability* 10, 2855.
- Dai, J., Ludois, D.C., 2014. Single active switch power electronics for kilowatt scale capacitive power transfer. *IEEE J. Emerg. Sel. Top Power Electron.* 3, 315–323.
- Dey, K.C., Yan, L., Wang, X., Wang, Y., Shen, H., Chowdhury, M., Yu, L., Qiu, C., Soundararaj, V., 2015. A review of communication, driver characteristics, and controls aspects of cooperative adaptive cruise control (CACC). *IEEE Trans. Intell. Transp. Syst.* 17, 491–509.
- EPA, U., 2013. US transportation sector greenhouse gas emissions: 1990–2011. Office of Transportation and Air Quality EPA-420-F-13-033a.
- FDOT, 2020. EV infrastructure master plan status report, <https://www.fdot.gov/planning/policy/ev/default>.
- Finance, B.N.E., 2021. Electric vehicle outlook 2021. Bloomberg Finance LP, Tech. Rep.
- Foundation, A.R.T., Company, M., 2014. Electric vehicles in Europe: gearing up for a new phase?.
- Gambella, C., Naoum-Sawaya, J., Ghaddar, B., 2018. The vehicle routing problem with floating targets: Formulation and solution approaches. *INFORMS J. Comput.* 30, 554–569.
- Gong, S., Du, L., 2018. Cooperative platoon control for a mixed traffic flow including human drive vehicles and connected and autonomous vehicles. *Transp. Res. B Methodol.* 116, 25–61.
- Gong, S., Shen, J., Du, L., 2016. Constrained optimization and distributed computation based car following control of a connected and autonomous vehicle platoon. *Transp. Res. B Methodol.* 94, 314–334.
- González, J.M., Sánchez, N.C., Llop, P.G.M., Pastor, L.A., Larson, K., 2021. Dynamic V2V power-sharing for collaborative fleets of autonomous vehicles, in: 2021 IEEE Electrical Power and Energy Conference (EPEC). pp. 408–413.
- Guanetti, J., Kim, Y., Borrelli, F., 2018. Control of connected and automated vehicles: State of the art and future challenges. *Annu. Rev. Control* 45, 18–40.
- Hannon, K., 2021. Could Roads Recharge Electric Cars? The Technology May Be Close [WWW Document]. The N.Y. Times.
- Hao, X., Lin, Z., Wang, H., Ou, S., Ouyang, M., 2020. Range cost-effectiveness of plug-in electric vehicle for heterogeneous consumers: An expanded total ownership cost approach. *Appl. Energy* 275, 115394.
- Huang, S., He, L., Gu, Y., Wood, K., Benjaafar, S., 2014. Design of a mobile charging service for electric vehicles in an urban environment. *IEEE Trans. Intell. Transp. Syst.* 16, 787–798.
- Huang, Y., Kockelman, K.M., 2020. Electric vehicle charging station locations: Elastic demand, station congestion, and network equilibrium. *Transp. Res. D Transp. Environ.* 78, 102179.
- Joseph, P.K., Elangovan, D., 2021. An Optimized Wireless Power Transmission Coil Design for Vehicle-to-Vehicle (V2V) Charging Application, in: Advances in Automation, Signal Processing, Instrumentation, and Control. Springer, pp. 1459–1469.
- Kosmanos, D., Maglaras, L.A., Mavrovouniotis, M., Moschoyiannis, S., Argyriou, A., Maglaras, A., Janicke, H., 2018. Route optimization of electric vehicles based on dynamic wireless charging. *IEEE Access* 6, 42551–42565.
- Li, J., 2019. NIO Charging Car to Help Power Up Other EVs in China [WWW Document]. Equalocean.
- Liang, K.-Y., Mårtensson, J., Johansson, K.H., 2015. Heavy-duty vehicle platoon formation for fuel efficiency. *IEEE Trans. Intell. Transp. Syst.* 17, 1051–1061.
- LLC, A.P., 2019. ORCA Inceptive data sheet [WWW Document]. URL www.andromedapower.com.
- Lu, G.J., Zhou, Y.P., 2013. A electric vehicle with bottom lateral linkage battery swapping and its battery swapping devices. CN 201310164242.X.
- Ma, H., Chu, L., Guo, J., Wang, J., Guo, C., 2020. Cooperative adaptive cruise control strategy optimization for electric vehicles based on SA-PSO with model predictive control. *IEEE Access* 8, 225745–225756.
- Maglaras, L.A., Topalis, F. V., Maglaras, A.L., 2014. Cooperative approaches for dymanic wireless charging of electric vehicles in a smart city, in: 2014 IEEE International Energy Conference (ENERGYCON). pp. 1365–1369.
- Masson, R., Lehuédé, F., Péton, O., 2014. The dial-a-ride problem with transfers. *Comput. Oper. Res.* 41, 12–23.

- Mayer, H.M., 1961. Final Report, Chicago Area Transportation Study.
- Miller, C.E., Tucker, A.W., Zemlin, R.A., 1960. Integer programming formulation of traveling salesman problems. *J. ACM (JACM)* 7, 326–329.
- Mobi EV Charger [WWW Document], n.d. FreeWire. URL <https://freewiretech.com/products/mobi-ev/>.
- Morris, C., 2021. BoostEV is an on-demand mobile EV charging network, like UberEats for hungry EVs [WWW Document].
- Mou, X., Zhao, R., Gladwin, D.T., 2019. Vehicle-to-Vehicle charging system fundamental and design comparison, in: 2019 IEEE International Conference on Industrial Technology (ICIT). pp. 1628–1633.
- Mou, X., Gladwin, D.T., Zhao, R., Sun, H., Yang, Z., 2020. Coil design for wireless vehicle-to-vehicle charging systems. *IEEE Access* 8, 172723–172733.
- Muelas, S., LaTorre, A., Peña, J.-M., 2013. A variable neighborhood search algorithm for the optimization of a dial-a-ride problem in a large city. *Expert Syst. Appl.* 40, 5516–5531.
- Nezamuddin, O., dos Santos, E.C., 2020. Vehicle-to-Vehicle In-Route Wireless Charging System, in: 2020 IEEE Transportation Electrification Conference & Expo (ITEC). pp. 371–376.
- Ngo, H., Kumar, A., Mishra, S., 2020. Optimal positioning of dynamic wireless charging infrastructure in a road network for battery electric vehicles. *Transp. Res. D Transp. Environ.* 85, 102385.
- NIO, n.d. NIO Power [WWW Document]. Nio. URL https://www.nio.com/de_DE/nio-power.
- Özbaygin, G., Karasan, O.E., Savelsbergh, M., Yaman, H., 2017. A branch-and-price algorithm for the vehicle routing problem with roaming delivery locations. *Transp. Res. B Methodol.* 100, 115–137.
- Parragh, S.N., 2011. Introducing heterogeneous users and vehicles into models and algorithms for the dial-a-ride problem. *Transp. Res. Part C Emerg. Technol.* 19, 912–930.
- Parragh, S.N., Doerner, K.F., Hartl, R.F., 2010. Variable neighborhood search for the dial-a-ride problem. *Comput. Oper. Res.* 37, 1129–1138.
- Parragh, S.N., Schmid, V., 2013. Hybrid column generation and large neighborhood search for the dial-a-ride problem. *Comput. Oper. Res.* 40, 490–497.
- PlugShare, 2022. PlugShare [WWW Document]. URL <https://www.pluginshare.com/>.
- Raeisi, R., Zografos, K.G., 2020. The electric vehicle routing problem with time windows and synchronised mobile battery swapping. *Transp. Res. B Methodol.* 140, 101–129.
- Reyes, D., Savelsbergh, M., Torriello, A., 2017. Vehicle routing with roaming delivery locations. *Transp. Res. Part C Emerg. Technol.* 80, 71–91.
- Roberts, B., Akkaya, K., Bulut, E., Kisacikoglu, M., 2017. An authentication framework for electric vehicle-to-electric vehicle charging applications, in: 2017 IEEE 14th International Conference on Mobile Ad Hoc and Sensor Systems (MASS). pp. 565–569.
- Ropke, S., Cordeau, J.-F., Laporte, G., 2007. Models and branch-and-cut algorithms for pickup and delivery problems with time windows. *Networks: An Int. J.* 49, 258–272.
- Schneider, M., Stenger, A., Goeke, D., 2014. The electric vehicle-routing problem with time windows and recharging stations. *Transp. Sci.* 48, 500–520.
- Shao, S., Guo, S., Qiu, X., 2017. A mobile battery swapping service for electric vehicles based on a battery swapping van. *Energies (Basel)* 10, 1667.
- Stabler, B., Bar-Gera, H., Sall, E., 2018. Transportation networks for research core team.
- Tang, P., He, F., Lin, X., Li, M., 2020. Online-to-offline mobile charging system for electric vehicles: Strategic planning and online operation. *Transp. Res. D Transp. Environ.* 87, 102522.
- Ucer, E., Buckreus, R., Kisacikoglu, M.C., Bulut, E., Guven, M., Sozer, Y., Giubbelini, L., 2019. A flexible v2v charger as a new layer of vehicle-grid integration framework, in: 2019 IEEE Transportation Electrification Conference and Expo (ITEC). pp. 1–7.
- Ulrich, L., 2021. How Is This A Good. EV Battery Swapping [WWW Document], Idea?
- Umesh, B.S., Khadikar, V.M., Zeineldin, H., Singh, S., Otrok, H., Mizouni, R., 2021. Direct Electric Vehicle to Vehicle (V2V) Power Transfer Using On-board Drivetrain and Motor Windings. *IEEE Trans. Ind. Electron.*
- Wang, Z., Wu, G., Barth, M.J., 2018. A review on cooperative adaptive cruise control (CACC) systems: Architectures, controls, and applications, in: 2018 21st International Conference on Intelligent Transportation Systems (ITSC). pp. 2884–2891.
- Wu, S., Xiong, R., Li, H., Nian, V., Ma, S., 2020. The state of the art on preheating lithium-ion batteries in cold weather. *J. Energy Storage* 27, 101059.
- Xie, J., Nie, Y., Liu, X., 2018. A greedy path-based algorithm for traffic assignment. *Transp. Res. Rec.* 2672, 36–44.
- Yan, L., Shen, H., Kang, L., Zhao, J., Xu, C., 2020. Reinforcement Learning based Scheduling for Cooperative EV-to-EV Dynamic Wireless Charging, in: 2020 IEEE 17th International Conference on Mobile Ad Hoc and Sensor Systems (MASS). pp. 401–409.
- Zanjani, A., Pinjari, A., Kamali, M., Thakur, A., Forecaster, S.T.D., Systematics, C., Short, J., Mysore, V., Tabatabaei, S.F., 2015. Estimation of statewide origin-destination truck flows using large streams of GPS data: Application for Florida statewide model, in: Proceedings of the 94th Annual Transportation Research Board Conference.